SECURITY CLASSIFICATION OF THIS PAGE

AD-A266 926

REPORT DOCUMENTATION PAGE

Form Approved OMB No. 0704-0188

1b. RESTRICTIVE MARKINGS	DISTRIBUTION STATEMENT A
2b. DECLASSIFICATION/DOWNGRADING SCHEDULE N/A	3. DISTRIBUTION/AVAILABILITY OF REPORT: Approved for public release; Distribution Unlimited UNLIMITED DISTRIBUTION
4. PERFORMING ORGANIZATION REPORT NUMBER(S)	5. MONITORING ORGANIZATION REPORT NUMBER(S) N/A
6a. NAME OF PERFORMING ORGANIZATION Company Name: SPACE EXPLORATION ASSOCIATES	6b. OFFICE SYMBOL (If applicable) N/A
7a. NAME OF MONITORING ORGANIZATION DARPA U.S. Army Missile Command	
6c. ADDRESS (City, State, and ZIP Code) Company Address: 141 W. Xenia Ave. P.O. Box 579 Cedarville, OH 45314	7b. ADDRESS (City, State, and ZIP Code) AMSMI-RD-WS-DP-SB Redstone Arsenal, AL 35898-5248
8a. NAME OF FUNDING/SPONSORING ORGANIZATION DARPA	8b. OFFICE SYMBOL (If applicable)
9. PROCUREMENT INSTRUMENT IDENTIFICATION NUMBER Contract # DAAH01-93-C-R031	
8c. ADDRESS (City, State, and ZIP Code) 3701 Fairfax Drive Arlington, VA 22203-1714	10. SOURCE OF FUNDING NUMBERS PROGRAM ELEMENT NO.: N/A PROJECT NO.: N/A TASK NO: N/A WORK UNIT ACCESSION NO: N/A

11. TITLE (Include Security Classification)
DIAMOND p-n JUNCTION COLD CATHODE UNCLASSIFIED

12. PERSONAL AUTHOR(S)
E.B. Kennel, R. Ya. Kucherov, C.R.W. Svensson

13a. TYPE OF REPORT	13b. TIME COVERED	14. DATE OF REPORT (Year, Month, Day)	15. PAGE COUNT
Final	FROM 11/30/92 TO 06/25/93	1993 June 29	46

16. SUPPLEMENTARY NOTATION

17. COSATI CODES		
FIELD	GROUP	SUB-GROUP

18. SUBJECT TERMS (Continue on reverse if necessary and identify by block number)
Cold Cathode, Negative Electron Affinity

19. ABSTRACT (Continue on reverse if necessary and identify by block number)

This effort successfully demonstrated that intercalated graphite fibers are outstanding cathode materials. Such fibers are stable in air at ambient temperature and offer current densities of over 100 Amps/cm^2 at 10 volts bias voltage (at 700 K). Ambient temperature cathodes also offer high current capability at somewhat higher bias voltage. Cesiated graphite and diamond both exhibit these characteristics, but graphite intercalation compounds are stable in air whereas the diamond/cesium system is not. The graphite cathodes DO NOT REQUIRE a cesium reservoir in order to function.

93-15986

93 7 5

20. DISTRIBUTION/AVAILABILITY OF ABSTRACT	21. ABSTRACT SECURITY CLASSIFICATION
☒ UNCLASSIFIED/UNLIMITED ☐ SAME AS RPT ☐ DTIC USERS	UNCLASSIFIED
22a. NAME OF RESPONSIBLE INDIVIDUAL Tech Monitor	22b. TELEPHONE (Include Area Code) / 22c. OFFICE SYMBOL

DD Form 1473, JUN 86 Previous editions are obsolete SECURITY CLASSIFICATION OF THIS PAGE

INNOVATIONS CERTIFICATION
CONTRACT #DAAH01-93-C-R031

This is to certify that all innovations under the contract, including all innovations originating under subcontracts at any tier, have been completely identified and reported to the Government.

Elliot B. Kennel

29 June 93

Elliot B. Kennel, Vice President

Date

FINAL REPORT
DIAMOND p-n JUNCTION COLD CATHODE

CAAH01-93-CR031

29 June 1993

Defense Advanced Research Projects Agency
3701 North Fairfax Drive
Arlington VA 22203-1714

Elliot B. Kennel, Principal Investigator
Vladimir Z. Kaibyshev
Rafail Y. Kucherov
Alexander G. Lagunov
C. Robert Svensson
Space Exploration Associates
PO Box 579
Cedarville OH 45314-0579

Paul R. Davis
William A Mackie
Linfield Research Institute
900 S. Baker St
Mcinnville, OR 97128-6894

EXECUTIVE SUMMARY

This effort successfully demonstrated that intercalated graphite fibers are outstanding cathode materials. Such fibers are stable in air at ambient temperature and offer current densities of over 100 Amps/cm^2 at 10 volts bias voltage (at 700 K). Ambient temperature cathodes also offer high current capability at somewhat higher bias voltage.

The effect is now presumed to be the result of the formation of cesium intercalation compounds, which present positive cesium ions near the surface of the graphite cathode (oriented such that the graphitic planes are parallel to the emission direction).

Our original postulate was that the observed enhanced emission is due to a negative electron affinity condition, which can exist in diamond as well as graphite. This postulate is insufficient to explain the data.

We now believe that good results from diamond are due to the presence of graphitic inclusions between individual grains of diamond. These graphitic inclusions are able to interact with cesium.

Intercalated graphite is relatively stable in air for moderate durations and can be handled without difficult. Thus the cathodes we are describing *do not require* a cesium reservoir in order to function.

Long term stability against cesium leakage is an issue, but we believe that this can be simply handled by using higher voltage and only moderate temperatures in order to achieve the enhanced emission. Future research should concentrate on developing the performance at ~100 °C or less, with bias voltages of 100 volts or possibly a little higher.

We believe that vapor grown carbon fiber (VGCF), a new type of carbon fiber with highly graphitized annular structure, offers very good potential for cathode applications, because it is easily intercalated, has very high electrical conductivity, and is available in very small diameters (~10 microns or even less).

Technology is now being developed by a group in Russia to utilize micron-sized fibers in cathode arrays which could have definite applications for video displays. This technology could be adapted to the use of intercalated carbon fibers.

I.1. INTRODUCTION

The purpose of this effort was to obtain data on anomalously high electron emission from the cesium graphite and cesium diamond system, and to apply the results to the creation of cold cathodes for very compact video displays and other applications.

Previously emission in the range of tens to hundreds of amps per square centimeter had been observed with both graphite and diamond in a cesium atmosphere. The observed magnitude of the emission vastly exceeds what could reasonably be obtained from a normal cesiated surface; therefore it was hypothesized that the diamond and/or graphite substrates were contributing in an unexpected way to the emission current.

Our original hypothesis was that the high emission was due to the creation of negative electron affinity surfaces, with electron injection from a p-type material.

Negative electron affinity occurs when the potential barrier due to the bandgap of a semiconductor is smaller than the electronic work function. In this case, it is possible for electron emission to occur with no additional input of energy.

Diamond, especially the 111 surface is a natural negative electron affinity cathode. Graphite, in the c direction (perpendicular to the graphitic planes), can also become a negative electron affinity cathode, but only in the presence of cesium or some other low work function material. Our original attempt to explain the observed anomalous emission was that electrons were being injected from the substrate and emitted through a negative electron affinity facet on the surface of the cathode.

Further, because of the fact that natural (bare) diamond is an NEA material, it was hoped that an NEA cathode could be fabricated without cesium. It is recognized that it is highly desirable to eliminate the presence of cesium in the system, because of the high costs that this would inevitably entail. Cesium is highly corrosive and must be kept free of oxygen, which generally means that it must be used only in systems which are very clean. Normally such systems must be outgassed in a 10^{-6} to 10^{-8} Torr vacuum. Cesium also tends to corrode many metals and ceramics. Thus a great deal of effort was spent on attempting to find alternatives to cesium.

Our simple model has been proven incorrect. We were unable to obtain exceptional results with bare diamond on n-type silicon. Furthermore, in the case of cesiated graphite, electron emission in the c-direction (which has the highest band gap) does not exceed normal expectations. However, in the a-b directions, the emission from cesiated graphite is extremely high. In these directions, the electron conduction modes are thought to be metallic. Thus, the situation with oriented graphite is exactly the opposite of what we had originally predicted.

Thus, we have been forced to amend the original hypothesis. We now believe that the high emission is caused by the presence of positive cesium ions in the graphitic lattice, which causes a local suppression of the electronic work function. In the diamond system, high emission can occur due to cesium intercalation of the graphitic inclusions, which exist between the polycrystalline grains.

Results from the cesium-pyrographite system showed definitively the presence of very high electron emission. About 110 A/cm^2 were achieved with a bias voltage of only 4 volts. This occurred with a temperature of 720 K. At 540 K, emission of about 32

A/cm^2 was obtained at the same bias voltage. Needless to say, these emission values are extraordinary. These results are presented here for the first time.

The very high currents obtained in these experiments are totally unexpected on the basis of thermionic or field emission and contain the following anomalous features:

a. The current rises linearly with respect to voltage, rather than showing a plateau due to saturation.

b. Visually, when the applied voltage is switched on, the current starts at a low level and then rises by around 10-20%. This effect occurs in about one second, and with the equipment on hand it was not possible to capture the effect on film. We interpret this as very strong ionic heating of the cathode.

c. The effect is about an order of magnitude higher when the graphite is used as the cathode; i.e., when electrons travel from the graphite to the metal (molybdenum) electrode. Interesting effects are also observed when the electrode pair is biased the other way, but the effects are much smaller.

Similar results have been obtained by colleagues at the Kurchatov Institute in Moscow.

II. THEORETICAL DISCUSSION OF NEA CONCEPT

In investigating a short arc discharge in a cesium plasma with graphitic and diamond-graphitic electrodes, we had previously discovered that at comparatively low voltages ~5-10 volts and at temperatures of ~600-900 K, the emission current reached 50 to 180 A/cm^2, which is impossible to explain considering the high ohmic resistances of the electrodes. According to our original hypothesis, the possible reason for such a high current density is negative electron affinity, which absolutely occurs in diamond (the vacuum work function is ~4-4.5 eV, in cesium vapor ~1.6 eV, the width of the forbidden zone is 5.5 eV) and is possible with graphite in cesium vapor. However, graphite in cesium vapor represents an extremely complex intercalated structure with cesium atoms between closely packed crystal planes of carbon. The processes that take place in them require special investigations.

Therefore, here we will only consider the case of a diamond NEA cathode. Figure 2.1 shows an energy diagram for a cathode with negative electron affinity.

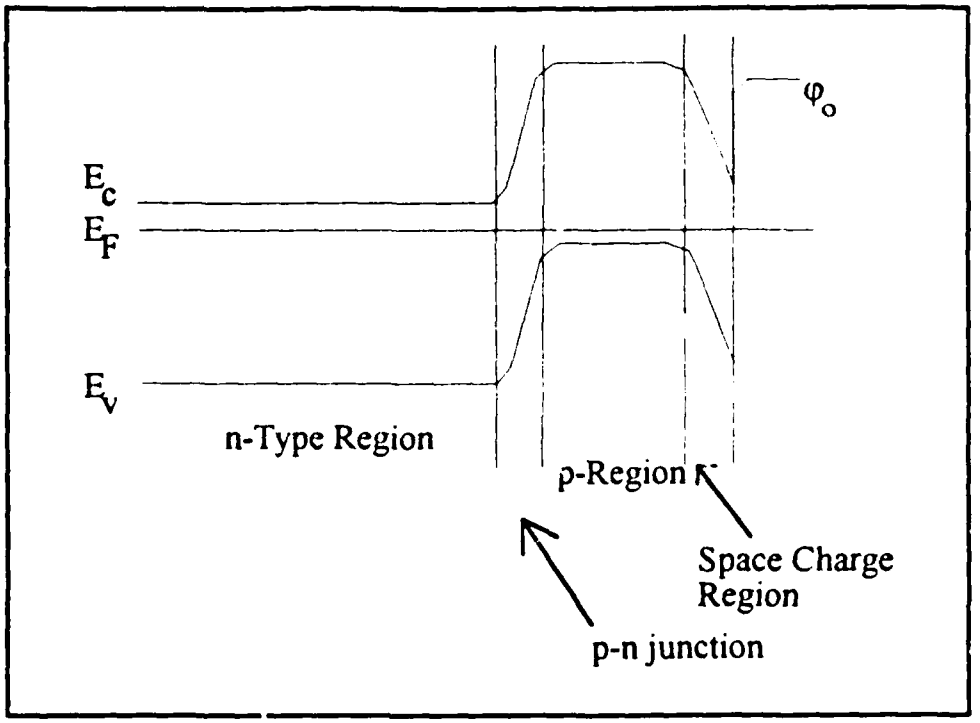

Figure 2.1.a. Energy Diagram of NEA Cathode

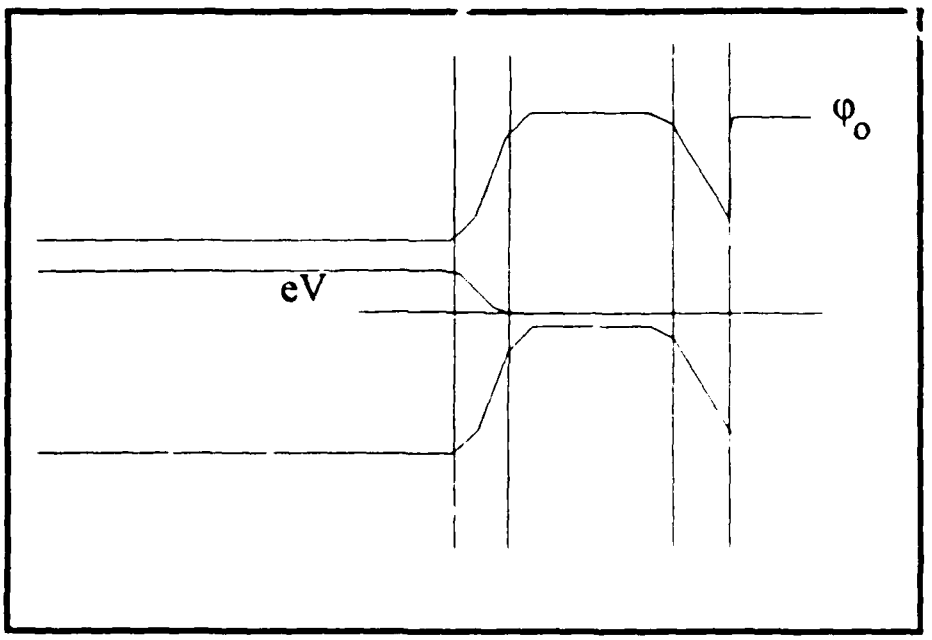

Figure 2.1.b. NEA Cathode Under Forward Bias

During the supply of a direct DC bias to an n-p transition, electrons from the zone of conductivity of a depleted n-type semiconductor pass into the zone of conductivity of a p-type semiconductor by overcoming the potential barrier. From here they diffuse to the cathode surface where by virtue of negative electron affinity they practically freely escape into the vacuum.

The required magnitude of the direct bias is provided by passing a current through the n-p transition. The total current in a semiconductor,

$$j = j_e + j_h, \tag{2.1}$$

has an electron j_e and a hole j_h component.

In NEA cathodes, the holes proceed to the cathode from the metallic contact at the emitter surface from where the hole current flows through the p-semiconductor p-n junction and further along the n-semiconductor to the opposite ohmic contact. An electrical diagram of such a device is shown in Figure 2.2.a. In this diagram the parallel vacuum diode through which the emission current flows is connected to an auxiliary circuit, thus discharging the electrons from the metallic contact.

A disadvantage of this design is the large ohmic resistance of the p-semiconductor which results in a non-uniform distribution of the hole current and the emission current at the semiconductor surface. These currents fall off rapidly in proportion to the distance from the junction. Therefore, the diameter of the emitting surface is usually 20-200 μm. With larger cathode sizes the contact must be similar to a thin metallic net with a fine mesh of a specified size.

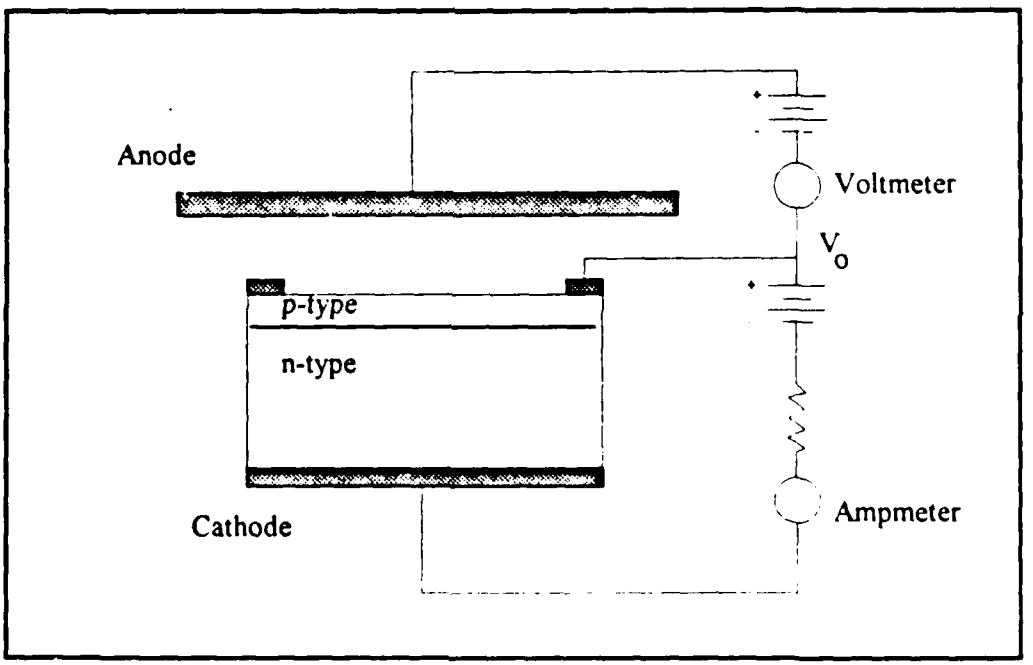

Figure 2.2.a. NEA Vacuum Cold Cathode

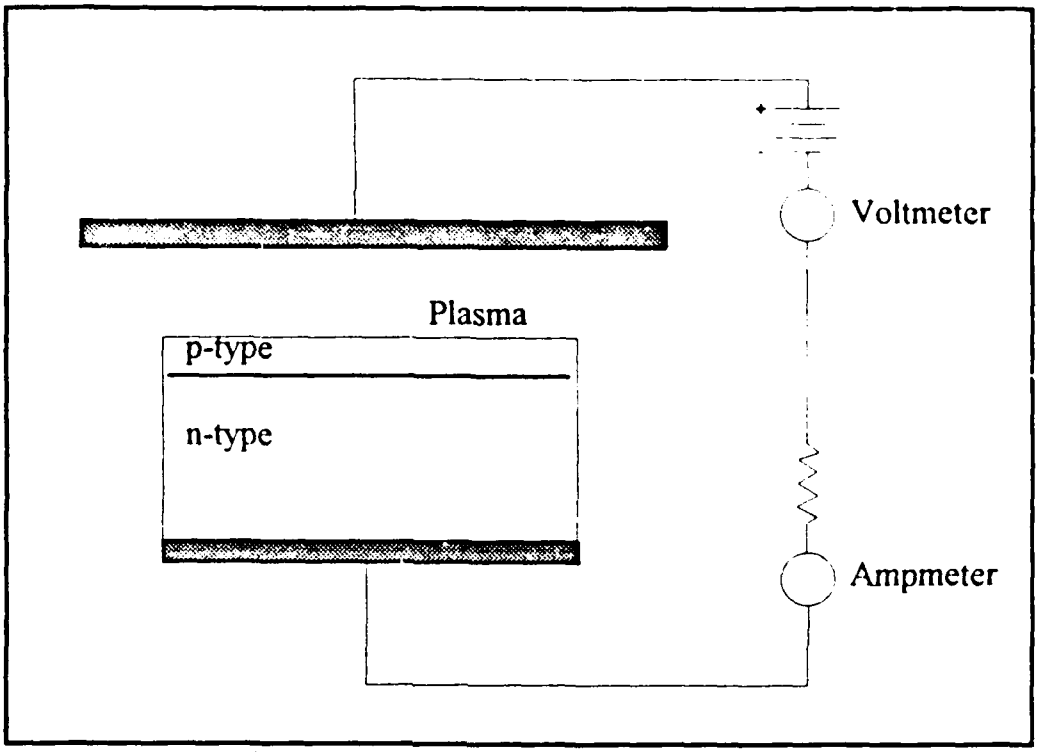

Figure 2.2.b. NEA Cathode for Plasma Device

In the operation of an NEA cathode with a plasma diode (Figure 2.2.b) emitter a hole current can be provided through processes of recombination of positive plasma ions at the cathode surface. At sufficiently high temperatures the holes at the cathode surface can also be generated by the departure of electrons from the cathode in the process of thermoelectric emission. Since the NEA cathode of a plasma diode can operate also without a metallic contact at its surface, this significantly simplifies its construction. In doing this, the size of the cathode is not limited.

However, it should be kept in mind that in this case the magnitude of the hole current is limited, which in turn can limit the emission current density.

An experimental NEA cathode is a p-semiconducting CVD diamond of the 111 type doped with boron, precipitated on a sublayer of monocrystalline n-type silicon. The emitting surface of the diamond is in contact with a gaseous plasma arc discharge and its work function is determined by the plasma composition. The application to the plasma diode of a voltage during the passage of a current through the heterostructure provides a positive bias at the n-p transition, the magnitude of which for a given emf of the source is determined by the resistances of the n and p semiconductors, the n-p transition, the gaseous plasma arc and the internal resistance of the current source.

The distinguishing characteristics of the device being considered are:

a. A high band-gap p-type semiconductor (diamond) serves as an electron emitter. The width of the forbidden zone of diamond is 5 5 eV, the work function of diamond is ~

4.2 eV. Thus, ΔE is ~1.3 eV and diamond is a natural NEA cathode, which in a number of situations does not require a special coating on a surface of lowered work function. The disadvantage of diamond is its high ohmic resistance. This is associated with the low degree of ionization, boron being the best known doping element with p diamond. At room temperature for doped (~10^{17} boron atoms/cm^3) diamond 111 the resistivity is greater than 10 ohm·cm. With an increase in temperature the ionization of acceptor boron atoms increases and the resistance drops off, but it still remains quite high, greater than 1 ohm·cm.

b. A relatively narrow-band semiconductor, n-type silicon, serves as a source of electrons. The use of a narrow-band semiconductor is a disadvantage of the NEA cathode, since for the effective injection of a significant electron current in the diamond a large bias voltage is required. At the same time, the use of silicon as a substrate in the CVD process permits the growth of a sufficiently good heteroepitaxial coating. Since recombination transitions in silicon are indirect, the diffusion length and life time of electrons in diamond are substantially greater than in other materials. This significantly reduces recombination losses.

The high resistance of the diamond film requires that at high current densities (~100 A/cm^2), the potential field in the semiconductor is 10^2 - 10^3 V/cm. This must be taken into account in describing the processes that take place in the cathode.

However, the question as to whether the structure obtained possesses "device quality" gives rise to doubt due to the significant disagreement in the lattice parameters (3.5669 for diamond and 5.4304 for silicon) and the large difference in the width of the active zone. Nevertheless, the results to date are difficult to interpret by not drawing upon a model of a cathode with negative electron affinity.

By neglecting end effects we will consider the one-dimensional problem of current flowing through this device. In order to simplify the problem, we will consider all contacts ohmic except the n-p transition.

The movement of the minority carrier charges (electrons) in a p-semiconductor is described by the following equation:

$$D_e \frac{d^2\Delta n}{dx^2} + \varepsilon\mu_o \frac{d\Delta n}{dx} - \frac{\Delta n}{\tau_n} \qquad (2.2)$$

where $x = 0$ corresponds to the location of the n-p transition; $n = n\text{-}n_0$ is the excess concentration of electrons; n_0 is the equilibrium concentration of electrons; $D_e = \frac{\mu_e kT}{q}$ is the electron diffusion coefficient; μ_e is the electron mobility; q is the elementary charge; T is the temperature τ_n is the electron life time, ε is the electrical field strength which under the conditions of our problem and with sufficient accuracy for this analysis can be assumed constant and equal to the voltage of the external field in the semiconductor.

The solution to this equation is in the form

$$\Delta n = A\exp\left(-\frac{x}{L}\right) + B\exp\left(-\frac{x}{L}\right) \tag{2.3}$$

$$\frac{1}{L} = \frac{1}{2L_n}\left[\left(\frac{\varepsilon}{\varepsilon_o}\right)^2 + 4\right]^{1/2} - \frac{|\varepsilon|}{2L_n\varepsilon_o} \tag{2.4}$$

where

$$L_n = \sqrt{D_n\tau_n} \quad \text{and} \quad \varepsilon_o = \frac{kT}{qL_n}$$

Since the only source of electrons is their injection in the n-p transition at x = 0, A = n(0) and B = 0. Hence,

$$\Delta n = \Delta n(0)\exp\left(-\frac{x}{L}\right) \tag{2.5}$$

As can be seen from equation (2.5), L, the so-called diffusion length, is the characteristic distance at which the nonequilibrium carrier concentration having arisen as a result of the injection decreases by a factor e. This decrease takes place as a result of recombination of excess non-equilibrium electrons with non-equilibrium holes. Thus qE_O corresponds to the energy acquired by the electrons in the field during passage through a distance equal to the diffusion length. If $\varepsilon << \varepsilon_O$, the weak field case, the electron current takes on basically a diffusive nature. For $\varepsilon >> \varepsilon_O$, the strong field case, the electron current is basically the conductance current.

In a weak field the inverse diffusion length equals $\frac{1}{L_n}$; and in a strong field

$$\frac{1}{L} = \frac{\varepsilon}{\varepsilon_o}\cdot\frac{1}{L_n} = \frac{q\varepsilon}{kT}$$

Since the electrical field in a semiconductor is approximately equal to j/σ (where j is the current, and σ is the conductivity) E_O decreases with an increasing conductivity, i e. with an increasing degree of doping and increase in temperature it falls off, and with an increase in current density, it increases. Figure 2.3 presents the current densities for which $E = E_O$ as a function of boron concentration in diamond.

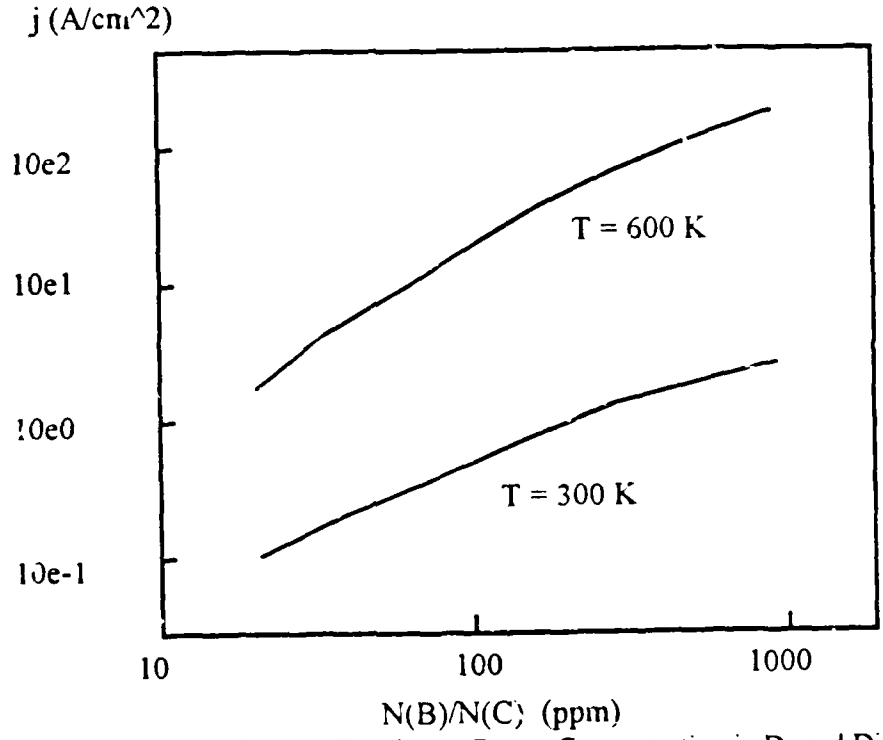

Figure 3. Dependence of Current Density on Boron Concentration in Doped Diamond

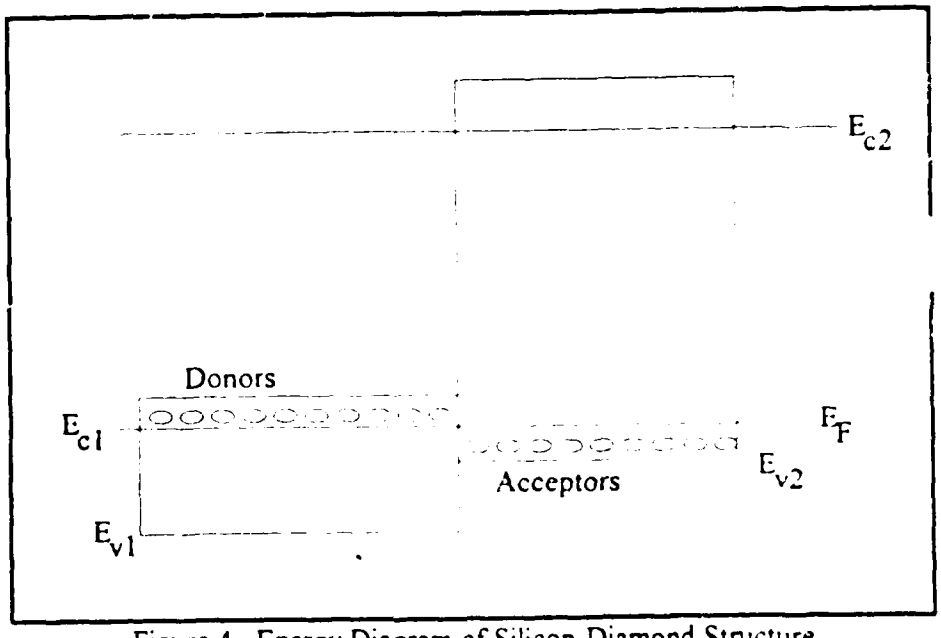

Figure 4. Energy Diagram of Silicon Diamond Structure

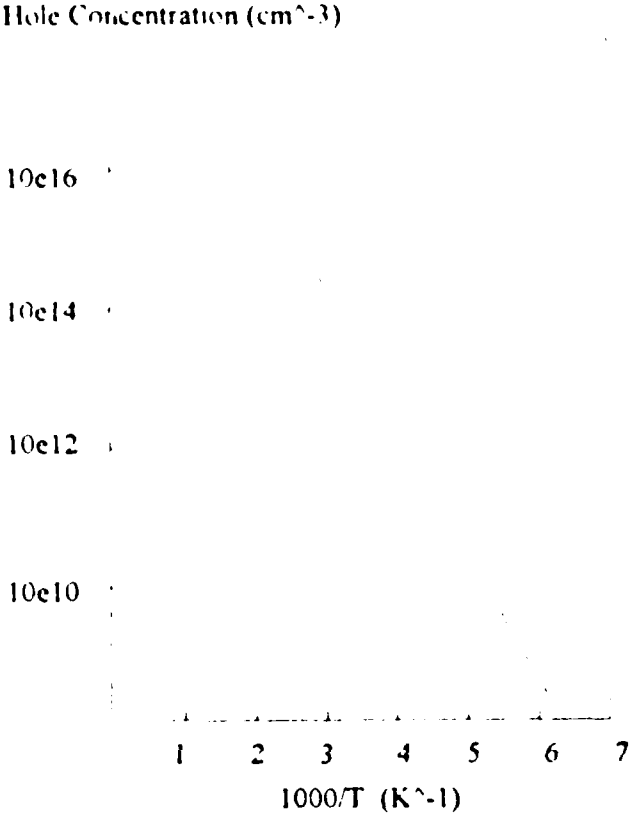

Figure 5 Hole Concentration as a Function of Temperature for Boron-Doped Diamond

Thus, at high current values ~10-10^2 A/cm^2 the diffusion length in diamond increases, which decreases recombination losses and allows the thickness of the p-semiconductor to be increased

The magnitude of the electrical current is

$$j_e = nq\mu_e\varepsilon + qD_e\frac{dn}{dx} = \left[q\mu_e\varepsilon + q\frac{D_e}{L}\right]n(0)\exp\left(-\frac{x}{L}\right)$$

Hence

$$j_e = j(0)\exp\left(-\frac{x}{L}\right) \qquad (2.6)$$

Since the vacuum level in an NEA p-semiconductor lies below the conductivity zone, in the absence of a potential barrier at the surface the emission current will equal

$$j_e^\circ = j_e(0)\exp\left(-\frac{t}{L}\right) \qquad (2.7)$$

where t is the thickness of the semiconductor

In the case when on the surface there are potential wells and recombination traps, the emission current decreases due to processes of surface recombinations of electrons captured in these wells and traps

$$j_e^\circ = j_e(0)\exp\left(-\frac{t}{L}\right)[1-R] \qquad (2.8)$$

where R is the ratio of the surface recombination current to the electron current having arrived at the surface. In the absence of thermionic emission and secondary electron emission at the cathode surface the total current in the gaseous plasma arc is equal to the cold cathode emission current plus the positive ion current arriving from the arc to the cathode surface.

$$j_e^\circ = j_e(0)\exp\left(-\frac{t}{L}\right)[1-R] + j_i \qquad (2.9)$$

VOLT-AMPERE CHARACTERISTICS OF HETEROTRANSITIONS

In contrast to models of n-p homotransitions proposed by Shockly (W. Shockly, Bell Syst Tech J 28 435 1949) that agree well with experiment, existing models of n-p heterotransitions do not permit an explanation of all phenomena that occur in them and they agree poorly with experimental data. This is associated with the fact that electrical properties at the boundary divisions depend strongly on the materials forming the heterotransition and on its fabrication technology.

The current flow mechanism in a heterotransition is determined by the profile of its energy region, the shape of which depends on the magnitude of the electron affinity, $\chi_{1,2}$, the work function, $\varphi_{1,2}$ and the width of the forbidden zone, $E_{g1,2}$ of each semiconductor. The shape of this profile is also influenced by lattice defects and foreign atoms at the semiconductor boundary divisions serving as captured electron traps or holes. The electrical charge at the boundary division leads to a substantial change in the shape of the barrier and the volt-ampere characteristic. The presence of the surface energy levels associated with surface traps leads also to recombination processes at the boundary division in the heterotransition

Diagrams of energy regions in different heterojunctions were proposed in the work of Anderson (R L. Anderson, Solid State Electronics 7 153 1962), neglecting the conditions at the boundary divisions Oldhom and Mills (W. J. Oldhom and A. J. Mills, Solid State Electronics 7 153 1964) studied the influence of these conditions. Nevertheless, as has been shown by experiments, the energy profiles obtained by Anderson prove to hold true for many heterotransitions.

In this diagram four types of n-p heterojunction profiles are possible (Figure 2 6) They arise as a function of the ratio between $\chi_{1,2}$, $\varphi_{1,2}$, $E_{g1,2}$, and the dielectric constants ε_1 and ε_2. (The subscript 1 pertains to the semiconductor with the smaller width of the forbidden zone)

We will utilize the Anderson profiles in order to evaluate the parameters of materials which could serve as n-semiconductors for the injection of electrons into p-diamond.

Let's initially examine n-silicon which will serve as the sublayer on which the diamond coating is produced.

The values of the indicated parameters for this case is given in Table II.1.

Table II.1 Semiconductor Band Properties.

Semiconductor	E_g	χ	φ
silicon	1.2 eV	4 eV	4.2 eV
diamond	5.5 eV	-0.7 eV	4.2 eV

The contact difference potential $\varphi_1 - \varphi_2$ in this case is equal to zero and the magnitude of the constituent barriers

$$\Delta E_0 = \chi_1 - \chi_2 = 4.8 \text{ eV} \quad ,$$

and

$$\Delta E_v = (\chi_1 + E_{g1}) - (\chi_2 - E_{g2}) = 0.1 \text{ eV} \quad .$$

Since $\varphi_1 - \varphi_2 = 0$ the gradient region is absent and the equilibrium profile of the energy region has a relatively simple shape (see Fig. 2.4), and the volt-ampere characteristic is described by the equation (R. L. Anderson):

$$j = j_e(0) + j_h(0)$$

$$= q\left\{N_{D1}\left(\frac{D_{e2}}{\tau_{e2}}\right)^{\frac{1}{2}} \exp\left(-\frac{q\Delta E_c}{kT}\right) + N_{A2}\gamma(T)\left[\frac{D_{p1}}{\tau_{p1}}\right]^{\frac{1}{2}} \exp\left(\frac{q\Delta E_v}{kT}\right)\right\}\left\{\exp\frac{qV}{kT} - 1\right\} \qquad (2.10)$$

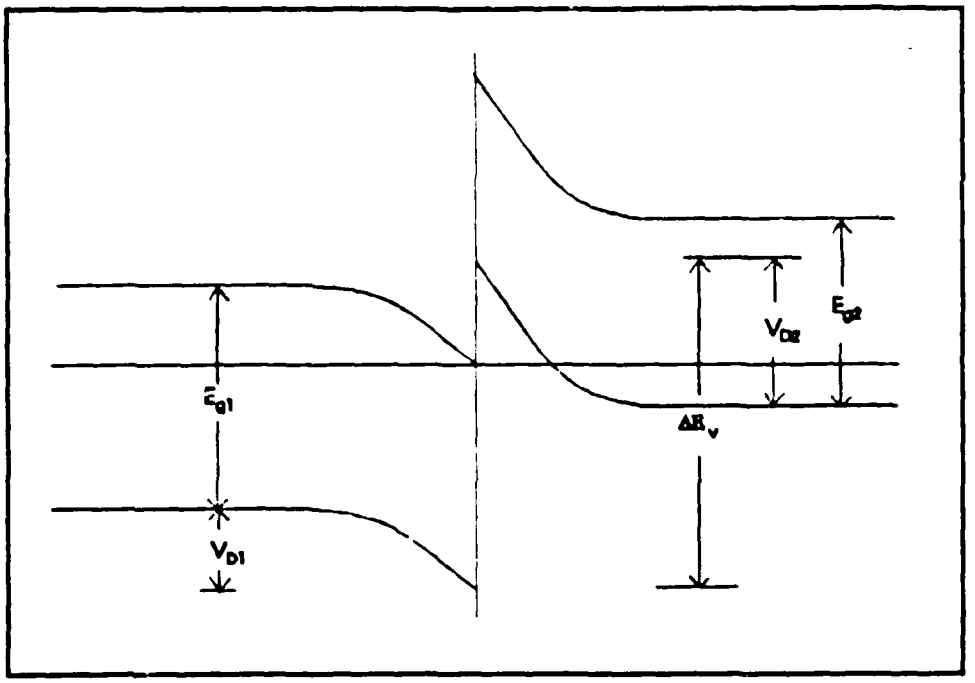

Figure 2.6.a. n-p Band Structure; $\chi_1 > \chi_2 + E_{g2}$, $\varphi_1 > \varphi_2$,

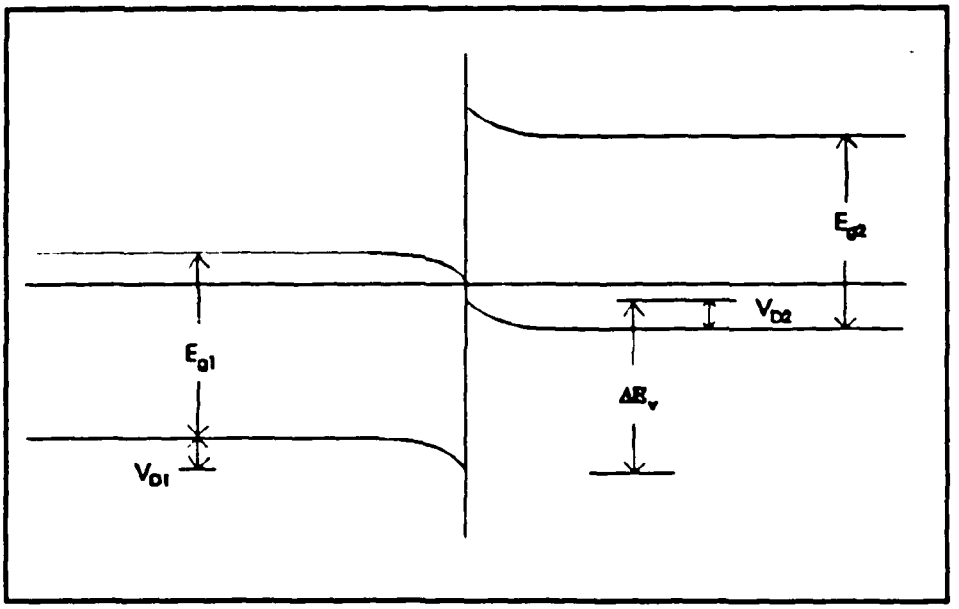

Figure 2.6.b. n-p Band Structure; $\chi_2 + E_{g2} > \chi_1 > \chi_2 + E_{g2}$, $\varphi_1 > \varphi_2$

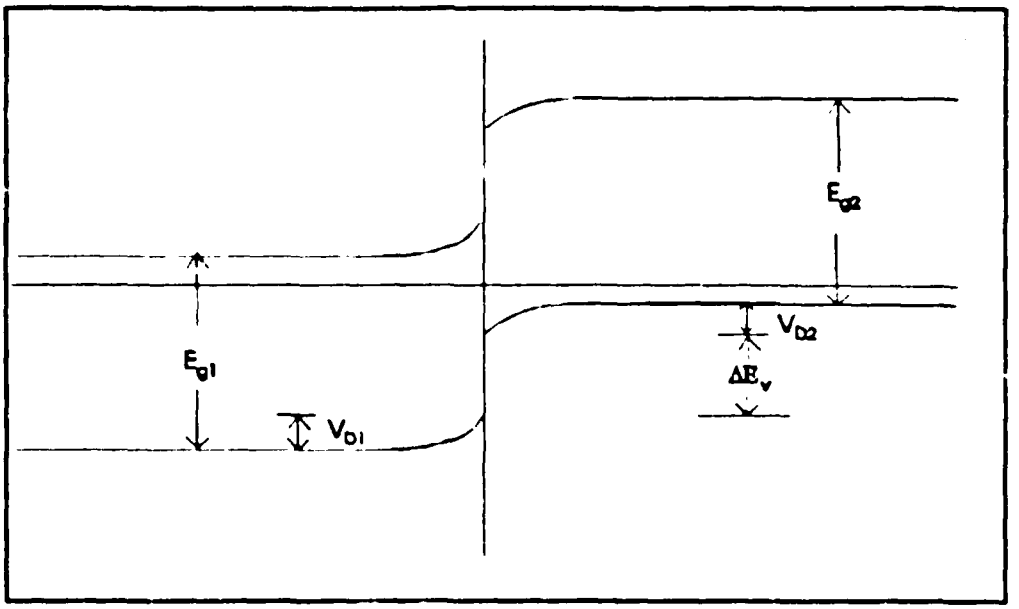

Figure 2.6.c. n-p Band Structure, $\chi_1 + E_{g1} > \chi_2 + E_{g2}$; $\chi_1 > \chi_2$; $\varphi_1 < \varphi_2$

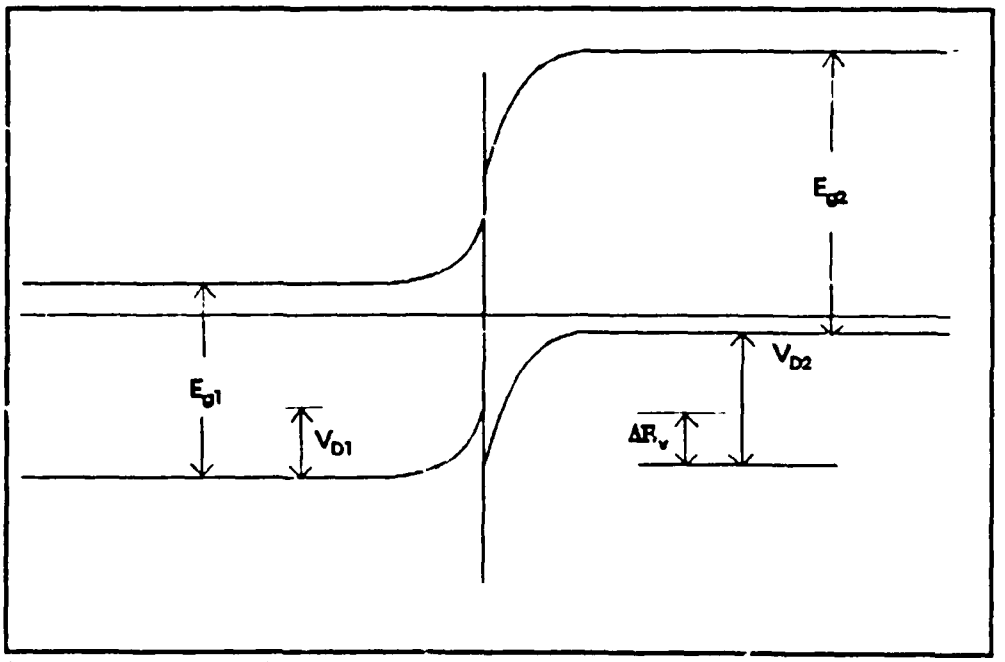

Figure 2.6.d. n-p Band Structure; $\chi_1 + E_{g1} < \chi_2 + E_{g2}$; $\chi_1 > \chi_2$; $\varphi_1 < \varphi_2$; $V_{D1} > \Delta E_v$

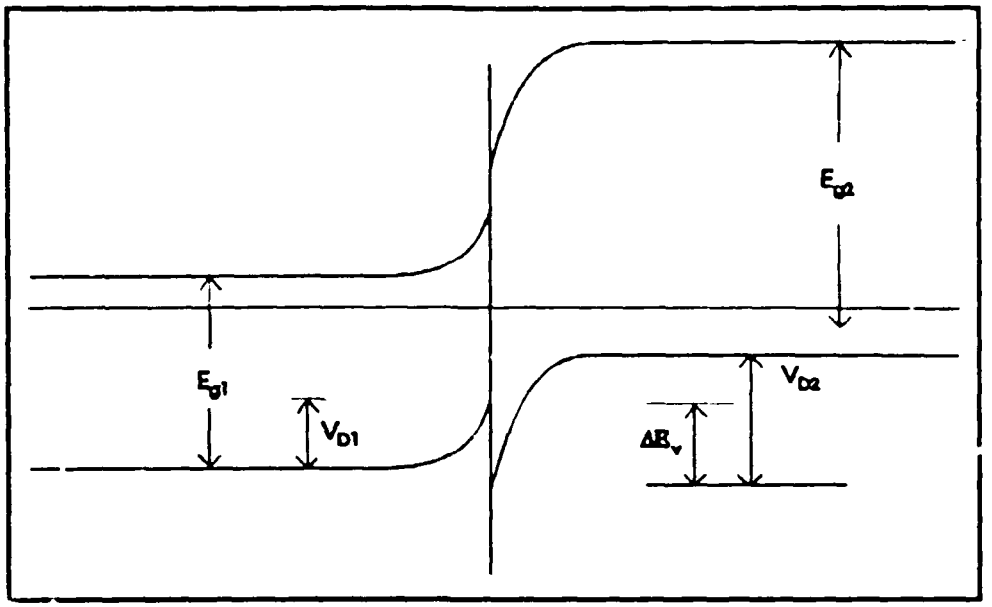

Figure 2.6.e. n-p Band Structure; $\chi_1 + E_{g1} < \chi_2 + E_{g2}$; $\chi_1 > \chi_2$; $\varphi_1 < \varphi_2$; $V_{D1} < \Delta E_v$

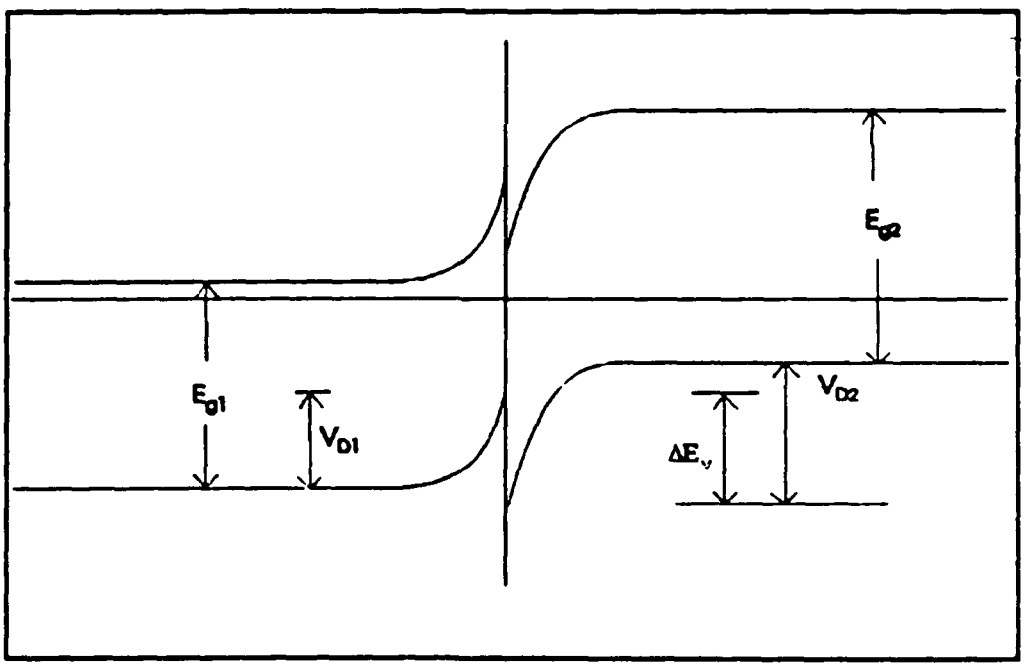

Figure 2.6.f. n-p Band Structure; $\chi_1 + E_{g1} > \chi_2$; $\chi_1 < \chi_2$; $V_{D1} > \Delta E_v$

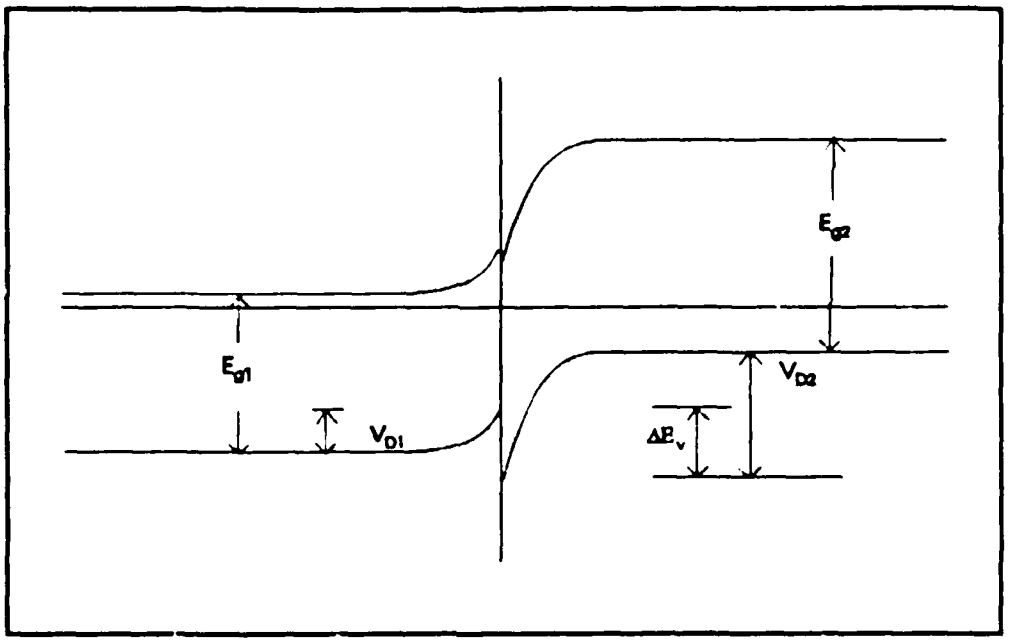

Figure 2.6.f. n-p Band Structure; $\chi_1 + E_{g1} > \chi_2$, $\chi_1 < \chi_2$, $V_{D1} < \Delta E_v$

where V is the bias voltage applied to the n-p transition; N_{D1} and N_{A2} are the concentrations of donor and acceptor constituents in silicon and diamond, respectively, and $\gamma(T)$ is the degree of ionization of boron atoms in II(σ) diamond $\gamma(T) = 2 \cdot 10^{-2}$ at room temperature and increases with increasing temperature.

$X \sim 10^{-2}$ is the barrier permeability (transmittancy) The ratio of the electron current to the hole current is

$$\frac{j_e}{j_h} = \frac{N_D}{N_{Dx}}\left[\frac{D_e\tau}{D_p\tau}\right]^{1/2} \exp\left[\frac{q}{kT}(\Delta E_c + \Delta E_v)\right] \qquad (2.11)$$

Because of the large differences in the width of the forbidden zones of diamond and silicon, the exponents at room temperature (being) ~200 and smaller, n-type silicon cannot serve as an electron injector for the diamond p-type semiconductor. In addition, due to differences in lattice constants, differing by ~40%, at the transition there arises a large number of surface conditions and defects that serve as recombination traps and which do not allow electron injection to be accomplished at the transition.

REQUIREMENTS FOR N-TYPE MATERIAL

Since n-type silicon cannot serve as an electron injector, we will examine other possible ways of forming an n-p heterotransition in the cathode under consideration.

Considering the technological process of forming diamond films, the materials which could form an n-semiconductor at the boundary with a p-diamond are the following: SiO_2, SiC, diamond-like carbon, and also n-diamond.

In order that an n-p transition can serve as an electron injector of a strong emitter it must satisfy certain requirements.

If the cold cathode emission sustains a hot discharge in a plasma diode, the electron emission current close to the cathode surface should exceed the ion current.

The ions recombining at the cold cathode surface is the source of holes in the p-semiconductor. As has been noted, due to recombination processes at the surface and during the travel of holes to the n-p transition, the hole current decreases by a factor

$$R = n_e(0)\exp\left[-\frac{l}{L}\right]$$

and the n-p transition electron current exceeds the emission current by the same magnitude. Therefore, the ratio $\frac{j_e}{j_h}$ in the n/p transition current significantly exceeds unity.

The volt-ampere characteristics of heterojunctions for different semiconductor pairs are described by equations similar to equation (10) but differ from it by terms that

take the gradient region into account.

In the general case, the characteristic is of the form:

$$j = q\left\{\left[\exp\left(\frac{qV}{kT}\right) - 1\right]\left[aN_{D1}\gamma_1 \exp\left(-\frac{\Delta E_c}{kT}\right) + bN_{A2}\gamma_2 \exp\left(-\frac{\Delta E_v}{kT}\right)\right]\right\} \qquad (2.12)$$

where a and b are multipliers that take into account charge mobility and the gradient region, and the ratio of electron current to hole current is equal to

$$\frac{j_e(0)}{j_h(0)} = \frac{a}{b}\frac{\gamma_1}{\gamma_2}\frac{N_{D1}}{N_{A2}}\exp\left[-\frac{q(\Delta E_c + \Delta E_v)}{kT}\right] \qquad (2.13)$$

This ratio should be greater than 1. Since the fundamental contribution to the magnitude of this ratio is made by the exponential multiplier, the semiconductor pair should approximately satisfy the condition:

$$K = \frac{q(\Delta E_c + \Delta E_v)}{kT} < 5 \qquad (2.14)$$

A decrease in K facilitates obtaining large emission currents in the NEA cathode, since the hole barrier that arises in the heterotransition reduces the hole current and decreases the necessary magnitude of ionization in the gaseous plasma arc.

Among the materials indicated above, silicon carbide, for which E=2.2 eV, does not satisfy condition (14). It is possible that n-type diamond could serve as an effective injector of electrons.

Based on data in SiO is a possible good injector of electrons for p-diamond. It is unclear, however, whether an oxide film existed on the silicon surface of the specimens used in the experiments and whether it was sufficiently high quality to serve as an injector.

The zonal structure and type of conductivity of diamond-like carbon or graphite, which in the specimens possibly exist as layers between silicon and p-diamond must also be considered. The question as to whether diamond-like carbon or graphite served as electron injectors in our tests remains open.

If in these tests graphite constituted a virtual cathode surface, then the large currents in these experiments can possibly be explained by high electron emission of graphite intercalated by cesium.

For the non-cesiated case, our experiments with the silicon-diamond system in hydrogen, nitrogen and argon plasmas can be explained entirely using the results of measuring the conductivity of diamond films carried out by Ting (Fig. 2.7). The magnitude of the currents obtained correlates with the hole conductivity of diamond and the shape of the oscillogram processes occurring in the n-p transitions and in the gaseous plasma arc (see Fig. 2.4). In the presence of a forward (DC) bias, the holes are initially retarded by

the barrier, but with an increase in voltage they freely pass into the silicon. In the presence of a reverse bias the electrons passing out of the gaseous plasma arc recombine with the holes at the surface of the NEA cathode, which now is the anode of the arc, and a hole current with an inverse reverse voltage arises.

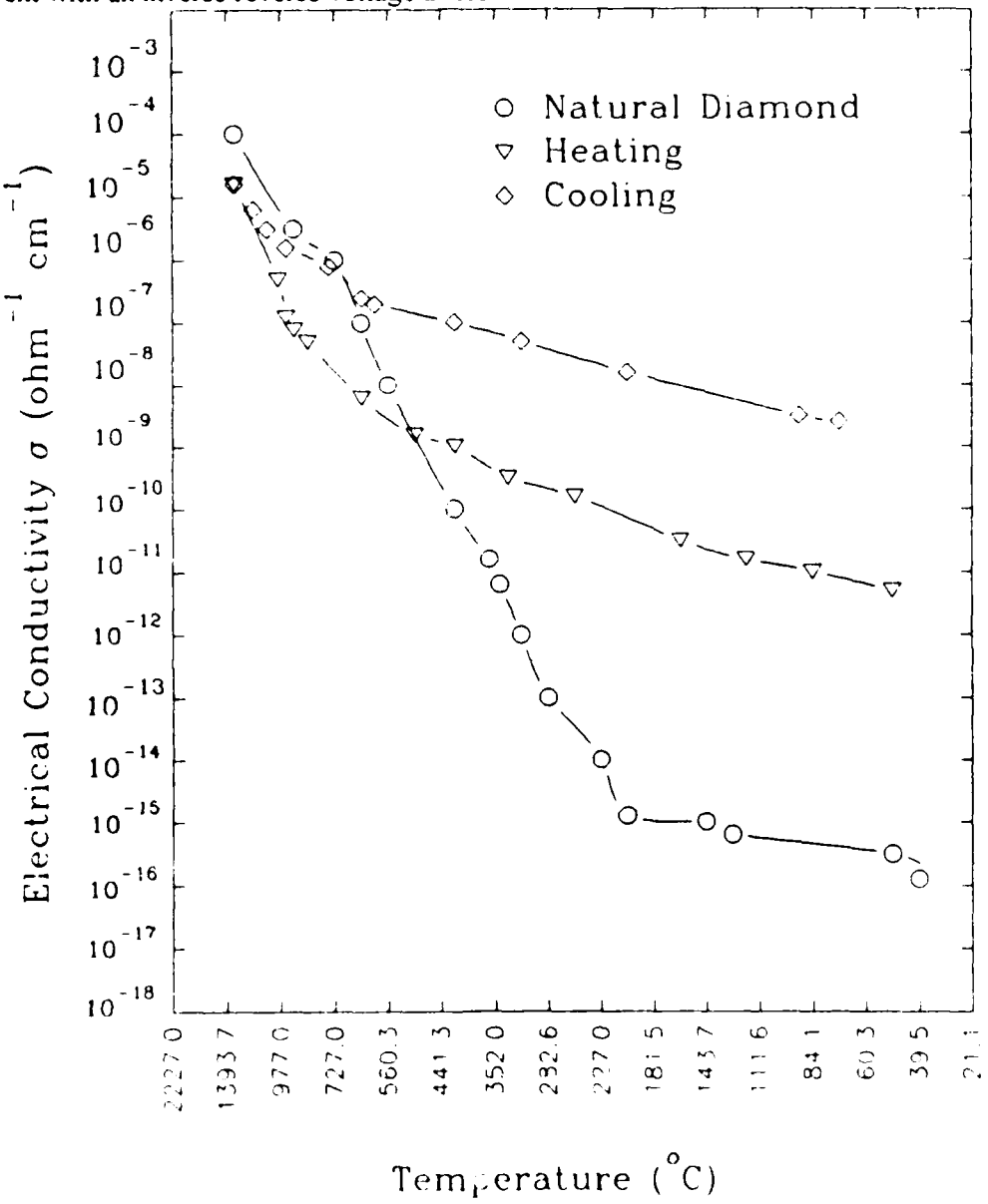

Figure 2.7. Electrical Conductivity of Diamond and Diamond-on-Carbon/Carbon

In summary, the model presented here is sufficient to explain all results for pure diamond and graphite in the absence of cesium. We were not able to extend the (high emission) results for the cesiated case to bare diamond under any circumstances. However, we did find extremely high emission for cesium graphite intercalation compounds when the electron emission is in the ab direction (parallel to graphitic planes).

INTERCALATION COMPOUNDS OF GRAPHITE

Intercalation compounds of cesium and graphite are formed by metal cesium ions forming a layer between the graphite atomic planes. These compounds typically exhibit a high range of order, as shown in Figure 2.8.

Note that the intercalation process tends to produce alternating rows of positive charges (due to the presence of cesium ions) and negative charges (from carbon electrons which are compensating for the cesium ions).

The following equilibrium reaction may be applied:

$$n_2\, C_{(n_1-1)}\, C_\alpha\, Cs + Cs \leftrightarrow (n_2+1) C_{(n_1-1)\alpha} Cs$$

where n is the number of graphite planes between the nearest laminar compounds; (n-1) is the carbon mole number in graphite layers which have the same distance between layers as the case of pure graphite, per mole of reactant; α is the carbon mole number in graphite layers which are filled with the reactant.

Oriented pyrolytic graphite serves as a basic material for the graphite-cesium source. Materials such as POCO are preferred, which are polycrystalline, but whose grains exhibit highly graphitic order with few defects. During intercalation, the graphite undergoes a uniaxial expansion along the crystallographic c-axis. Maximum expansion is achieved for C_8Cs at 1.78. This is shown in Figure 2.8.b.

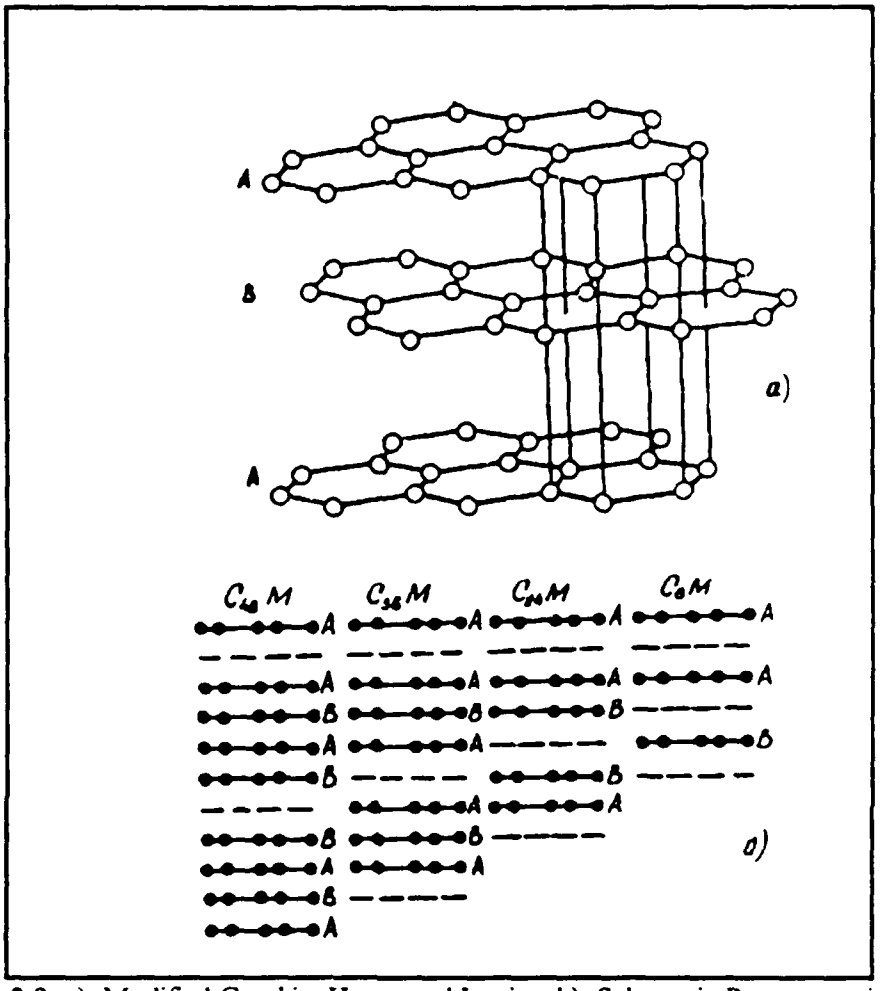

Figure 2.8 a) Modified Graphite Hexagonal Lattice; b) Schematic Representation of Phase Structures of the Cs-Graphite System

It is not known what the situation looks like at the surface of the graphite. We suspect, however, that positive Cs ions may be present at the surface. These positive ions (versus the normal neutral atom of adsorbed cesium present for a metal electrode) could create a very localized negative electron affinity, or at least a very low positive affinity, as shown in Figure 2.9.

Note that in the ab directions, the conductivity for graphite is metal-like. For this case the problem of electron injection is essentially eliminated.

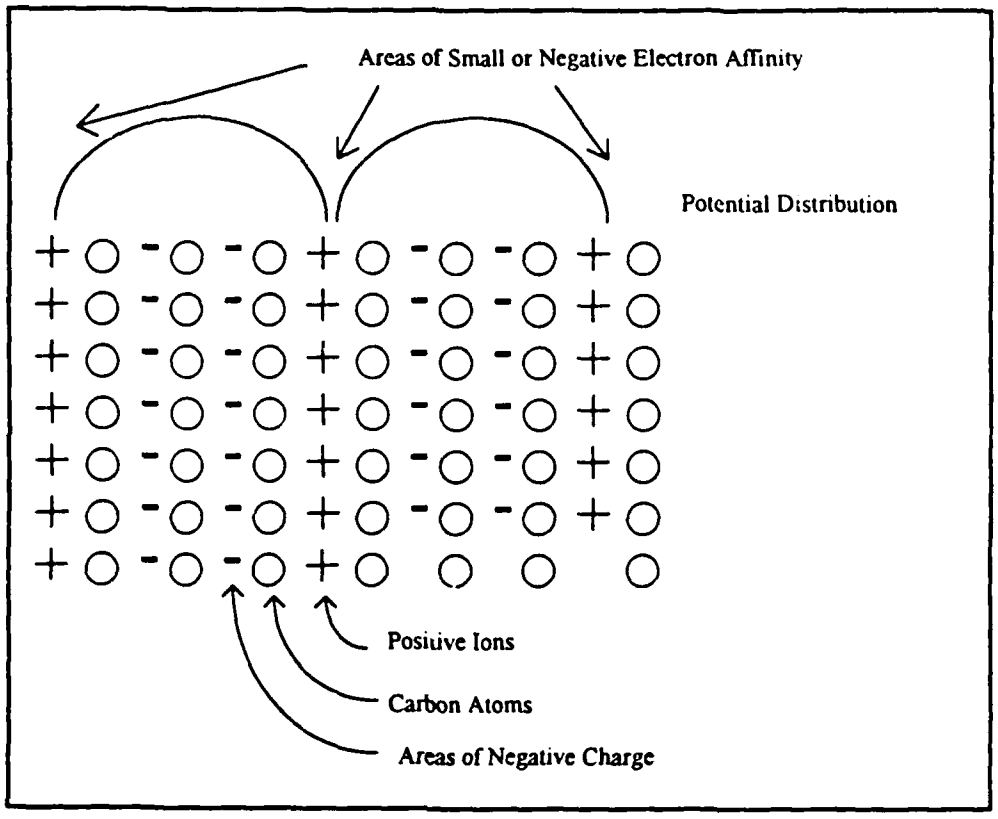

Figure 2.9. Hypothesized Potential Distribution in Cs-Graphite System

Bariated graphite, or intercalation compounds of some other metal ion, could serve the same function. Barium could be introduced either as an intercalant (this will require temperature of around ~1000 K in a sealed container in order to fabricate; more precise analysis is being carried out). We are also investigating the possible use of other metals.

Another possibility is to ion implant cesium or barium into the surface of the graphite. However, since the precise energy state of the cesium is probably important, we cannot be sure that ion implantation will yield the desired results.

Other materials which can be of interest include titanium diboride and possibly other composites.

Another possibility is to consider artificially manufactured superlattices which have similar patterns of alternating charge layers.

References.

1. W. Shockly, Bell Syst Tech. J. 28 435 1949

2. R.L. Anderson, Solid State Electronics 7 153 1962

3. W. J. Oldhom and A. J. Mills, Solid State Electronics 7 153 1964

4. J. M. Ting, internal memo, 1 May 93.

II. EXPERIMENTS WITH DIAMOND

The experiments with diamond showed the following characteristics

a Very poor reproducibility of high current emission in cesiated samples Maximum current varied widely from sample to sample, even if the samples appeared to be nearly identical

b No anomalous emission was reliably observed without the presence of cesium vapor

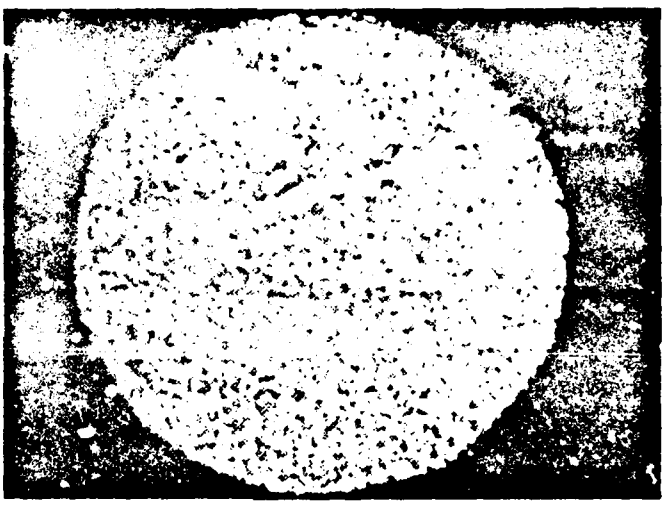

Figure 3 1 Diamond on Silicon Surface, Partial Coverage 25x Photo

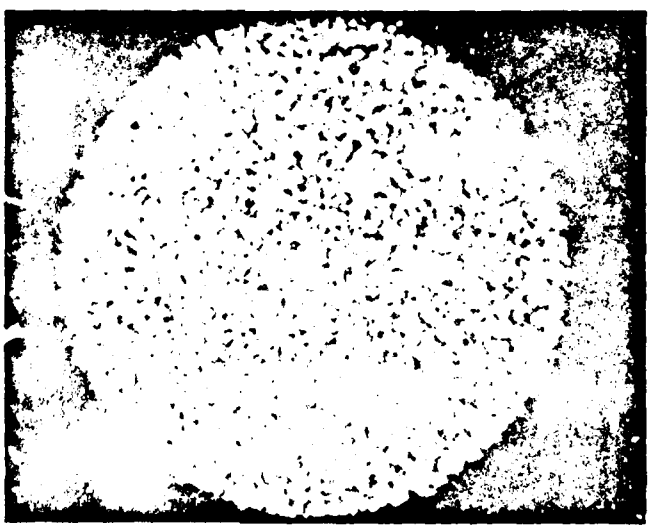

Figure 3 2 Diamond on Silicon Surface, Partial Coverage 100x Photo

CESIATED DIAMOND EXPERIMENTS

Experiments were also carried out in Sweden (Gothenburg University) on diamond cathodes and anodes fabricated by us. Experiments in Sweden were not funded by us, the results are reported here for the first time.

We fabricated a diamond cathode and tested it in a bell jar with flowing cesium present from the nominal anode. The anode was graphitized nickel (for reference purposes, we refer to the nickel electrode as the anode and the diamond electrode as the cathode, although the setup was tested biased in both directions).

The diamond film cathode was fabricated at 1220 K with a gas mixture of 99.5% and 0.5% methane. The base metal was molybdenum. Under these conditions, the diamond is expected to be preferentially oriented with the 111 face, which has the highest band gap (5.5 eV). It was our original assumption that this would result in enhanced emission.

The surface resistance was measured with a digital resistance meter, with a measuring voltage of less than 0.7 V. Two platinum wires with smooth ends were used as measuring probes. The resistance between the diamond layer and the clean molybdenum metal was approximately 85 kΩ as shown in the figure below. The resistance measured between two points and the diamond layer was approximately 170 kΩ (or twice that across the diamond layer), regardless of the probe position. Presumably this indicates that the current conduction path in the diamond is perpendicular to the surface, and there is not much surface conductivity.

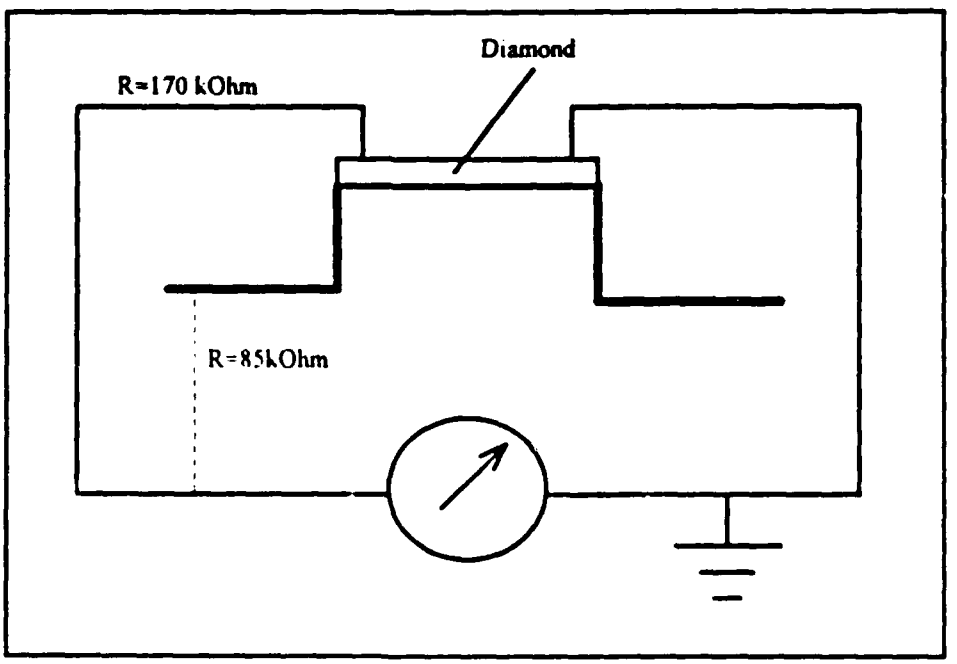

Figure 3.3. Resistance Measurements of Diamond Emitter

The reference experimental parameters are as follows T_{Cs} = 570 K, T_a = 670 K, and T_c = 1000 K. The sweep voltage ranged from 20 to -20 volts. Under these conditions, no significant electron current was observed.

After about 30 minutes, an electron current from the nickel electrode (nominal anode) to the diamond electrode was observed, as shown in Figure 3.2.

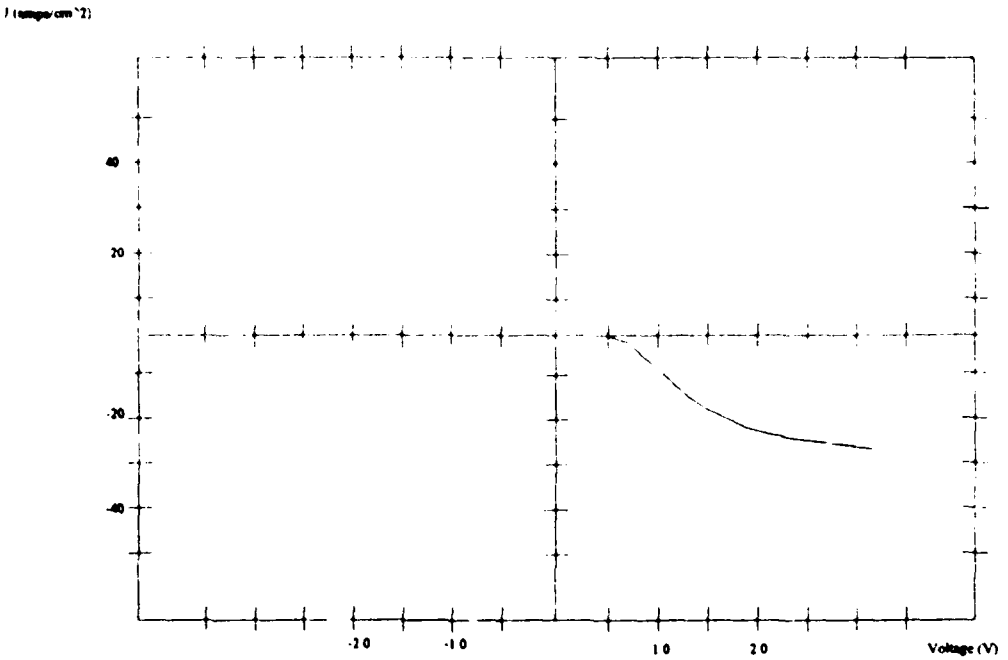

Figure 3.4. Back Current from Nickel/Graphite to Diamond

After three hours, the electron emission current from the diamond to the nickel/graphite electrode increased markedly, as shown in Figure 3. Optically, the diamond appeared to emit blue needle-like filaments of plasma.

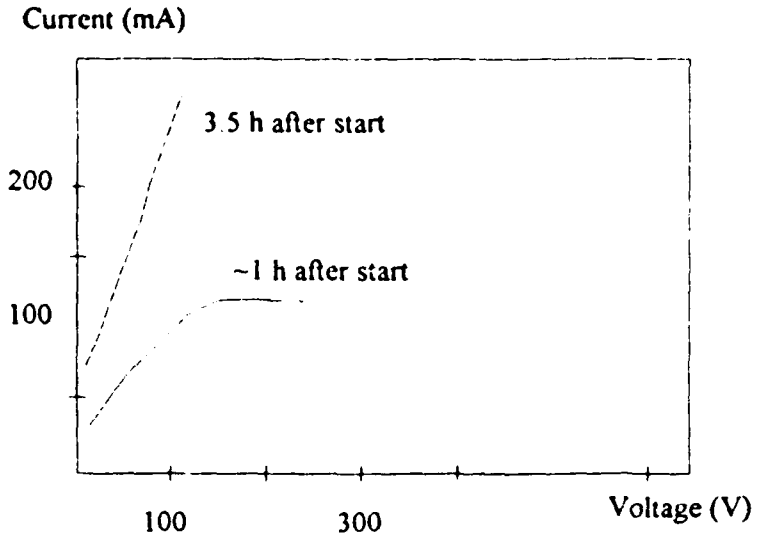

Figure 3.5. I-V Characteristic of Diamond Cathode

We interpret the change in emission current as being due to a slow reaction between cesium and graphitic inclusions in the diamond. The needlelike filaments are possibly due to emission from intercalated graphite compounds existing *between* the grains of diamond in our diamond film.

The diamond results are impressive, but not nearly as good as those achieved for intercalated graphite. Moreover, the diamond results reported here are at least an order of magnitude lower than we had achieved previously; and the high emission results for diamond are not achievable without the presence of cesium vapor in the bell jar.

Our interpretation is that the emission comes not from the bulk diamond as we had originally assumed, but from the graphitic inclusions between the individual crystals. If so, this would explain why the result is poorly reproducible, as the amount of graphitic inclusions is small to begin with (much less than one percent of the total carbon present), and probably varies widely from sample to sample even under carefully controlled conditions.

It should be noted that our high emission data came from diamond on silicon, in which the growth of diamond was not too thick; hence the resistance through the electrode was lower and more graphitic inclusions were present

ELECTRON EMISSION MICROGRAPHS

We were not able to obtain good electron emission micrographs.

We used a vacuum field emission cell to measure electron emission from a diamond on silicon specimen. In this cell, applied fields of 10^4 V/cm on a flat surface can be achieved. Presumably, a field enhancement could exit at the surfaces of the small-radius diamond crystals.

A schematic of the emission cell is shown in Figure 3.4. The cell consists of a phosphor-coated glass screen, for viewing the electron emission distribution which is spaced 1 mm away from the diamond film surface by Macor™ spacers. Not shown in the

figure is the structure which holds the assembly together. The cell is mounted in such a way that there is electrical contact with the Si substrate for the diamond film and with the phosphor screen. In operation, a positive bias is applied to the screen, and the silicon substrate is held at ground potential. An electrometer in the high voltage side of the circuit measures current emitted from the diamond film and collected at the screen.

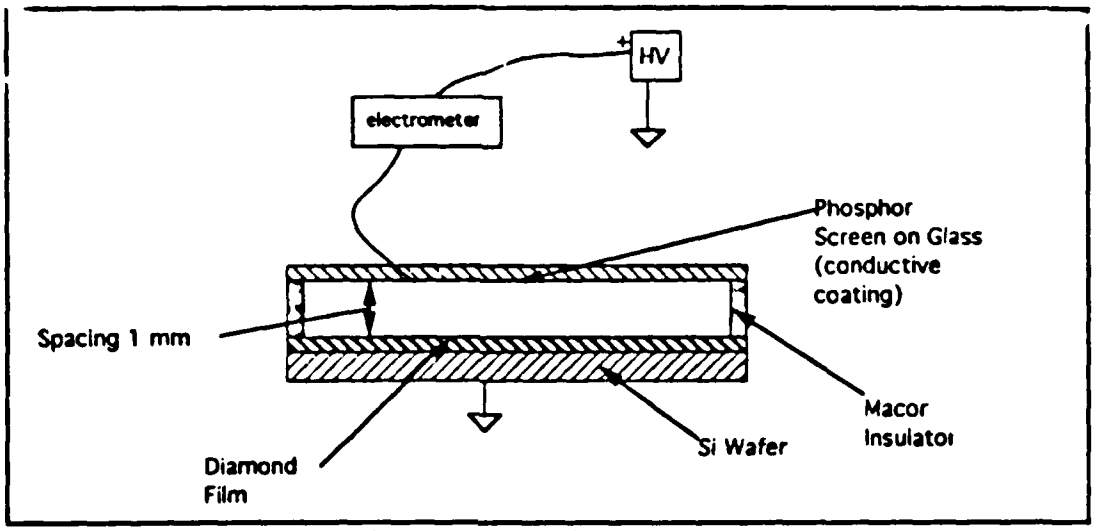

Figure 3.4. Experimental Setup

The specimen can be heated by passing current through a tantalum ribbon which is pressed against the silicon substrate. An iron/constantan thermocouple is spotwelded to the ribbon to monitor its temperature. Temperatures up to 500 °C are easy to establish and maintain by this means.

Figures 3.5-7 show data from diamond on silicon. Figures 3.5-6 are for an unheated sample, with successfully higher voltages applied to the cell. A maximum current of 10 nA was observed at the maximum applied voltage of 1750 V, corresponding to a parallel plate field of 1.75×10^4 V/cm. The data of Figure 3.7 were obtained in a similar fashion, while the specimen was heated to about 100 °C. These data are plotted in Fowler-Nordheim plots, (I/V^2) vs $1/V$.

An attempt was made to obtain higher currents from the specimen by operating the cell at higher voltages. A current of 1.25 μA was observed at a maximum applied voltage of 3.0 kV, with the specimen heated to 500 °C, as shown in Figure 3.8. There is clearly significant leakage current in this case as can be seen when the data are recast in the form of a V vs I plot (Figure 3.9) which shows a constant cell resistance of about 2×10^9 ohms.

Following this discovery, the emission was re-measured with the specimen cool but high applied voltages, obtaining a maximum emission current of 5 μA at an applied voltage of 2.3 kV. The data show Fowler-Nordheim behavior, as indicated in Figure 3.10, but with an offset (leakage) current, which is more clearly visible in the summary plot of Figure 3.11.

Higher temperature plots did not yield good results. This is probably due to the fact that the extremely small emission current is swamped by the leakage current, which also increases with temperature.

ANALYSIS OF DIAMOND EMISSION

The Fowler-Nordheim equation, which describes field emission of electrons from metal surfaces, can be written as

$$J = \left(\frac{C_1 F^2}{\phi}\right) \exp\left[-\frac{C_2 \phi^{3/2}}{F}\right] \tag{3.1}$$

where J is the emitted current density in A/cm^2, ϕ is the work function in eV, F is the applied field in V/cm, and C_1 and C_2 are positive and approximately constant, but include some slowly varying functions of F. For a fixed emitting area, we expect our measured I to be proportional to J (emitting area fixed) and we may write the field as

$$F = \beta V \tag{3.2}$$

where β is a constant field enhancement factor, equal to 1/d for a diode of spacing d.

Thus, a Fowler-Nordheim plot of $\ln(I/V^2)$ vs (1/V) should yield a straight line with slope

$$m = -\frac{C_2 \phi^{3/2}}{\beta V}, \tag{3.3}$$

that is, proportional to the work function to the 3/2 power and inversely proportional to the applied voltage.

The value of C_2 may be determined from first principles, but both the work function and the field enhancement factor are unknown in our case. The local field enhancement is very sensitive to roughness of the diamond film, both on the scale of the diamond crystal size (about 5 μm radius) and on the scale of the roughness of individual crystals (sub-micron). If we make the assumption that our measurement cell is simply a parallel-plate diode, then the field is just V/d, where d is the spacing, and we calculate a work function of the order of 0.05 eV for the specimen. This assumption is clearly unjustified, because the surface of the specimen is not smooth, but rather has a gross roughness of the order of 5 μm, the radii of the diamond particles. If we make the assumption (also not well-justified) that the local field is determined primarily by the radius of curvature of the diamond particles, then we derive a value of approximately 0.5

eV for the specimen work function. We might actually expect the local field at the surface of a diamond particle to be even greater than the second assumption used here, due to microscopic roughness of the diamond crystals, but it is not obvious how to estimate field enhancement due to this roughness.

It would be desirable to do a companion set of experiments, using a scanning Auger electron spectrometer (SAM) system to do retarding potential work function mapping of the surface, determining areas of relatively low and relatively high work function. It should be possible to clean the surface by ion sputtering in the SAM system, and verify directly the cleanliness of the surface thus prepared.

SUMMARY

The only high emission results with diamond occurred for the cesiated case. Attempts to obtain high emission from diamond in various plasmas (Ar, H_2, N_2, and air) were unsuccessful. In no case did we reliably observe emission higher from the diamond-on-silicon system compared to the bare silicon cathode.

Our high emission results from cesiated diamond varied widely from sample to sample for no apparent reason.

As described in Section IV, it now seems more likely that the high emission occurs as a result of positive ions held near the surface of a graphite intercalation compound. Perhaps it is possible to form such compounds with the miniscule graphitic inclusions which exist between individual diamond crystals.

In any case, the results obtained with graphite (Section IV) are much more reproducible and appear much more promising than those for diamond. Furthermore, the results with graphite intercalation compounds show that it is not necessary to have a cesium *plasma* present in the system; the intercalation compound is stable and can be handled in air.

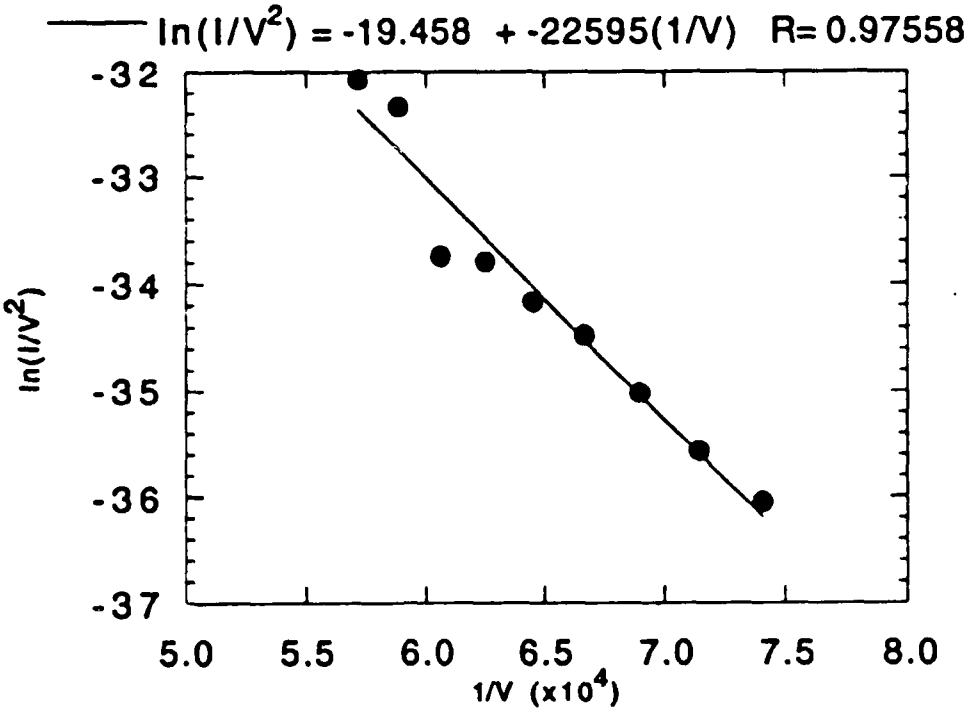

Figure 3.5 Ambient Temperature Fowler-Nordheim Plot.

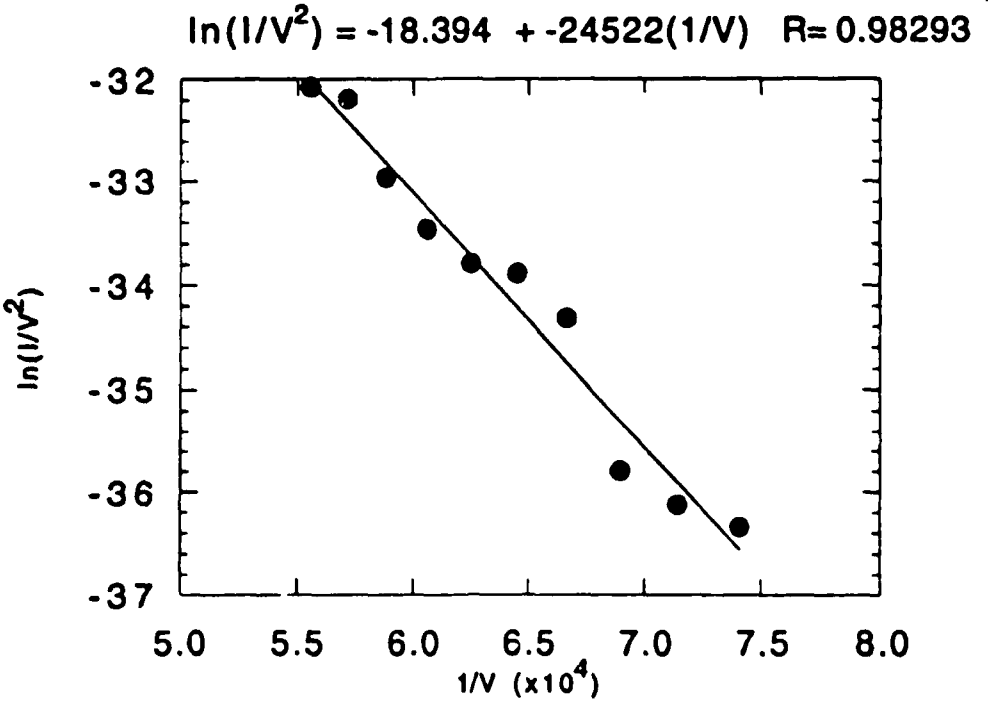

Figure 3.6 Ambient Temperature Fowler-Nordheim Plot (Run #2)

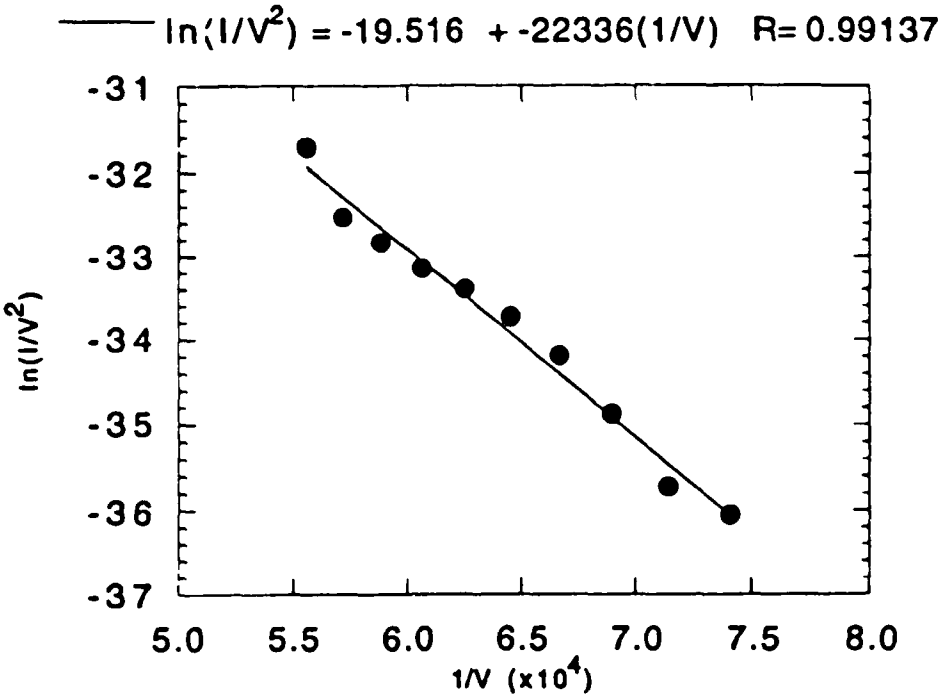

Figure 3.7 100 °C Fowler Nordheim Plot

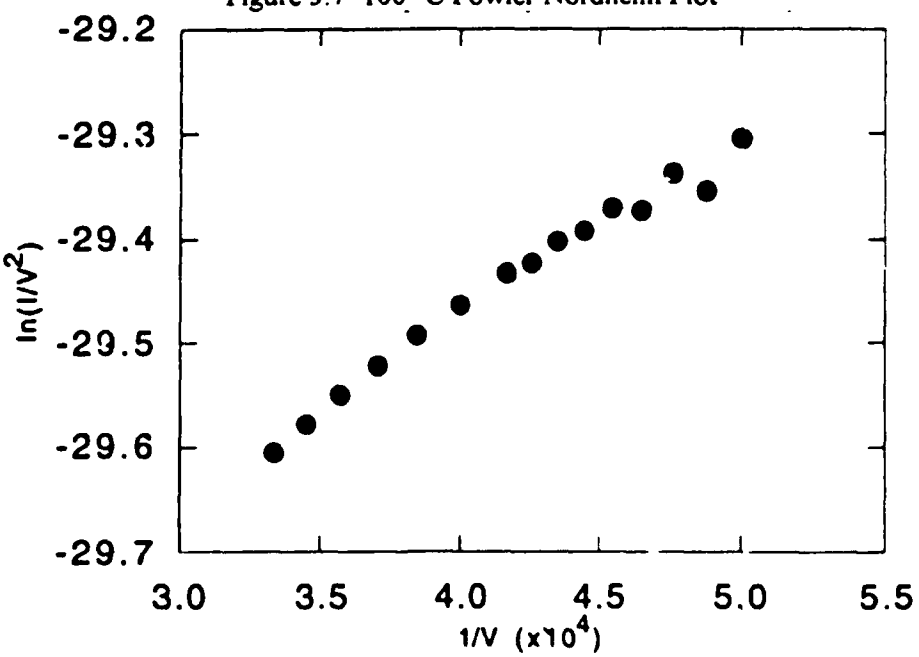

Figure 3.8 500 °C Fowler Nordheim Plot (Leakage Current)

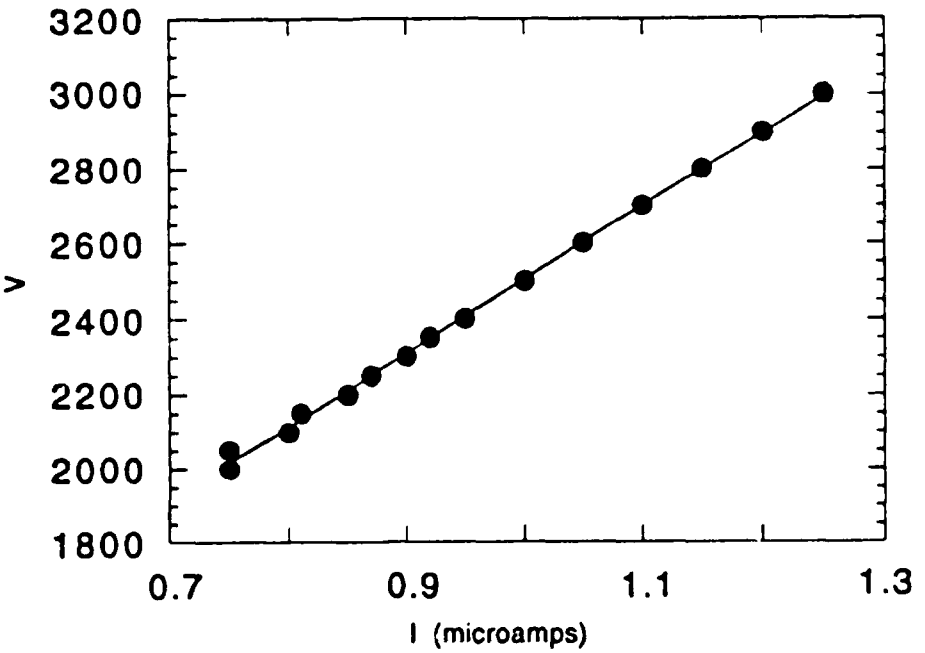

Figure 3.9 500 °C Ohm's Law Plot, R = 300 O

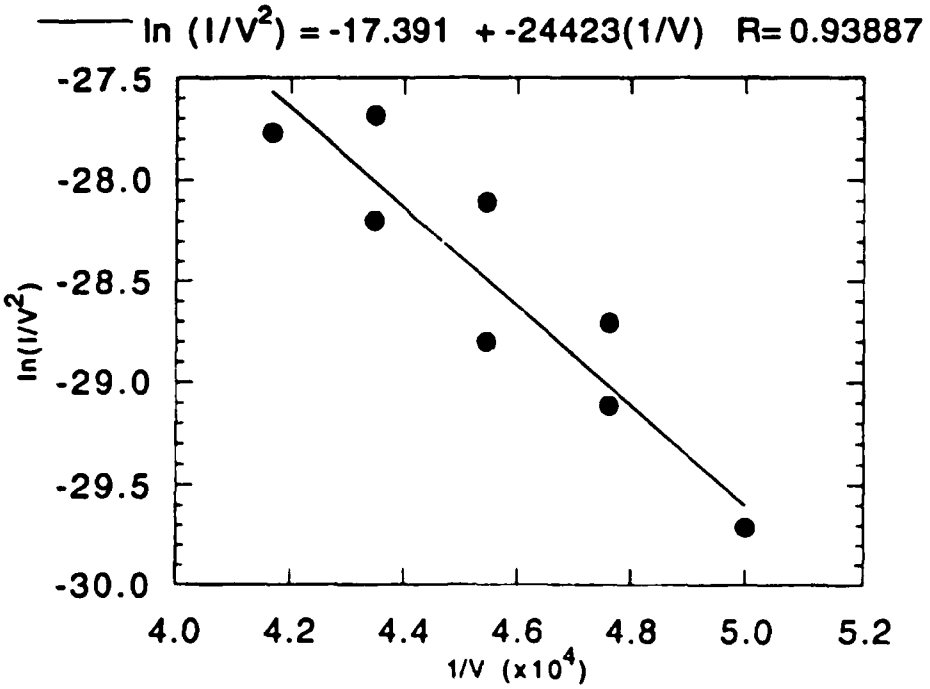

Figure 3.10 Ambient Temperature Fowler-Nordheim Plot, at Higher Voltage

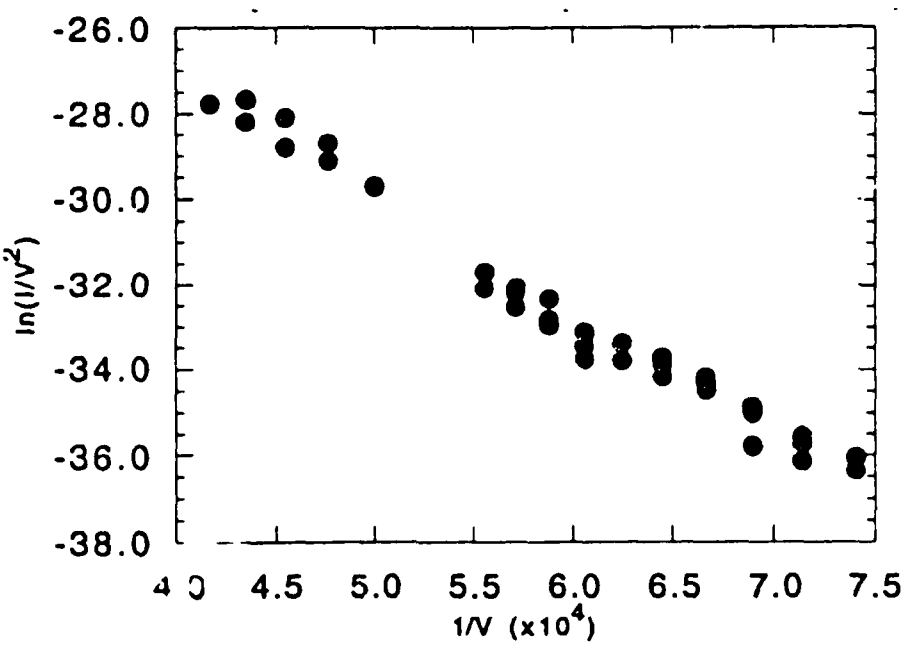

Figure 11. Composite of Fowler Nordheim Data. Higher Temperature Data Shows a Higher Leakage Current.

IV. INTERCALATED GRAPHITE RESULTS

Although positive results had been achieved both with cesiated diamond and cesiated graphite, we chose initially to emphasize diamond because it (seemingly) is a less complicated system than graphite. Because graphite is a metal in the ab planes and a p-type semiconductor in the c direction, and because graphite can form intercalation compounds with cesium, we felt that graphite/cesium would be too complicated a system to study. Furthermore, we felt that the most likely mechanism for the high emission which we have observed was negative electron affinity. In this case, diamond is a much stronger NEA cathode than graphite, and exhibits NEA characteristics in vacuum or even in air, whereas graphite only exhibits NEA characteristics with cesium or some other work function reducing surface additive.

This logic is well and good, but suffered from one problem--all of our experiments with non-cesiated diamond failed to produce beneficial results! We were unable to find any reproducible experimental evidence of non-classical emission in the absence of cesium. We were thus forced to consider the possibility that some other interaction involving cesium was responsible for the observed enhanced emission.

Thus, it was necessary to recheck our hypothesis by returning to the graphite-cesium system. By using a pyrolytic graphite specimen, it was possible to orient the electrode surface such that electron emission can occur either parallel to the ab planes, or perpendicular to them (i.e., in the c direction).

Experiments were carried out with a closed electrode pair to characterize electron emission and collection from a pyrolytic graphite electrode. The electrode consists of about 1 cm^2 of pyrolytic graphite. The graphitic planes were oriented parallel to the direction of electron emission.

When the graphitic planes were oriented perpendicular to the electron emission, no interesting results were achieved. Because the conduction mode in this direction is metallic (rather than semiconducting) this indicates that the high emission was not an effect of the band structure of carbon as we had initially hypothesized.

Our original experiments used colloidal graphite applied to a metal substrate. The surface structure contains high quality graphite, but with random orientation. We had assumed that the anomalous emission must be associated with a semiconductor effect and not with metallic conduction. Hence our negative electron affinity hypothesis (which seemed to be confirmed by cesiated diamond experiments) assumed that high emission must be occurring perpendicular to the graphite planes, in which case the material is behaving as a high-bandgap p-type semiconductor. However, the new data contradict this hypothesis.

The graphite was mechanically (spring-loaded) attached to a metal holder. Temperature measurement was accomplished using a thermocouple which was imbedded in the metal holder. Thus, there is a contact thermal resistance, which no doubt slightly distorts the results. No attempt was made to measure or correct for the temperature drop between the graphite and holder, owing to the difficulty of attaching thermocouples to the composite. It is supposed that the temperature difference was around ~50 K.

The results with pyrolytic graphite show the presence of very high electron emission, whereas we are unable to achieve impressive results with bare material. This is

not due simply to the lower work function of cesium, however, as the observed current is far in excess of what can normally be obtained from cesiated surfaces.

The observed emission has several unusual characteristics.

First, the emission has no discernible saturation point, but seems to demonstrate a linear resistance.

Second, ionic heating is observed visually, as the curve is deflected by roughly 30% after switching on the applied voltage in about a second.

Third, when operated in reverse mode (electron emission from the metal electrode to the graphite), anomalous emission is also observed, but at a factor of ten reduced current. This situation is shown in Figure 4.2.

Because of the difficulties we have had in obtaining anomalous emission in the absence of cesium, it is instructive to examine the structure of the graphite-cesium system a little more closely.

Intercalation compounds of cesium and graphite are formed by metal cesium ions forming a layer between the graphite atomic planes. These compounds typically exhibit a high range of order, as shown in Figure 4.3.b.

Note that the intercalation process tends to produce alternating rows of positive charges (due to the presence of cesium ions) and negative charges (from carbon electrons which are compensating for the cesium ions).

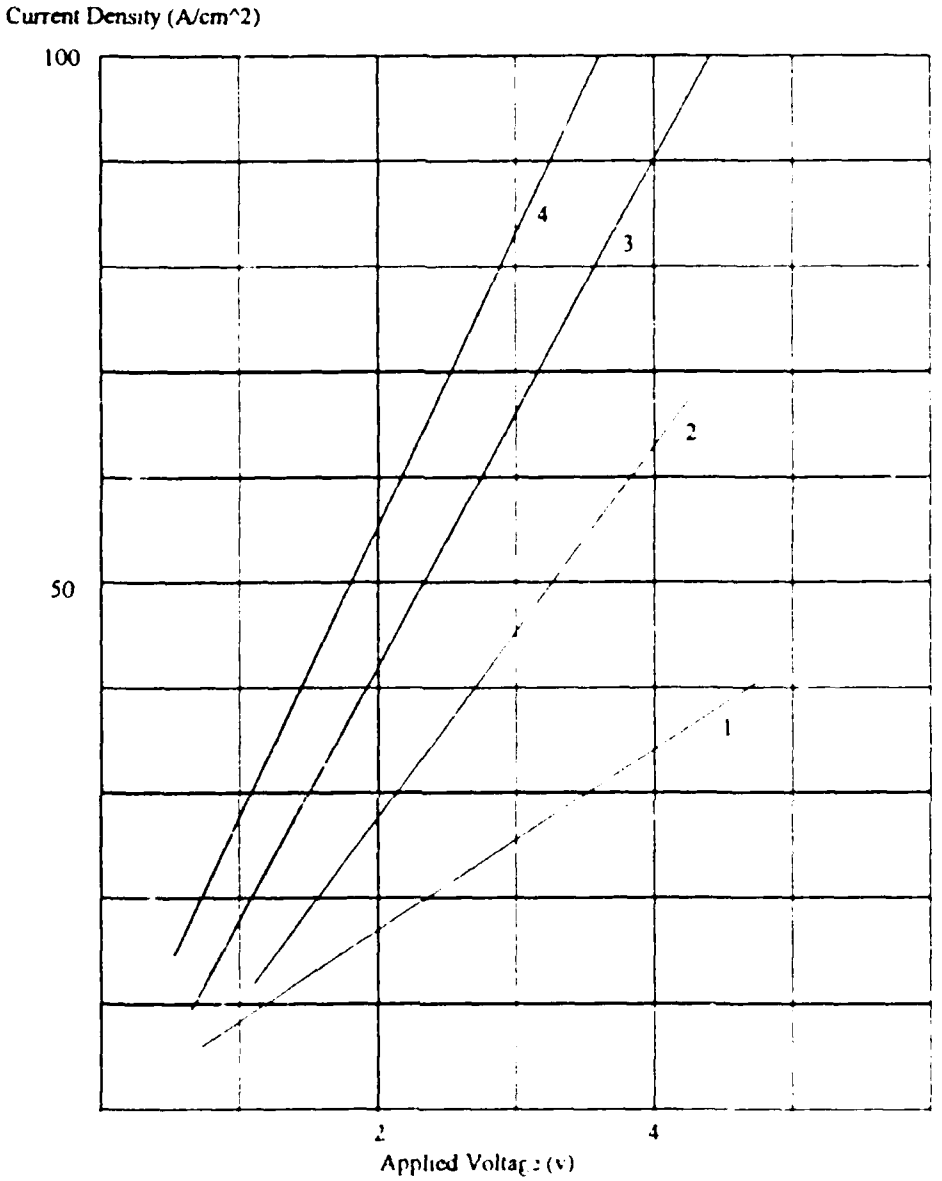

Figure 1. High Currents Observed with Cesiated Pyrographite

Table I. Parameters of Curves in Figure 1.

Curve	Electrode Temp	Equiv Cs Temp	P_{Cs} (Torr)
1	540	490	0.2
2	610	523	0.4
3	690	573	2
4	720	600	4

The following equilibrium reaction may be applied

$$n_2 C_{(n_1-1)} C_\alpha Cs + Cs \leftrightarrow (n_2 + 1) C_{(n_1-1)\alpha} Cs$$

where n is the number of graphite planes between the nearest laminar compounds, (n-1) is the carbon mole number in graphite layers which have the same distance between layers as the case of pure graphite, per mole of reactant, α is the carbon mole number in graphite layers which are filled with the reactant

Oriented pyrolytic graphite serves as a basic material for the graphite-cesium source Materials such as POCO are preferred, which are polycrystalline, but whose grains exhibit highly graphitic order with few defects During intercalation, the graphite undergoes a uniaxial expansion along the crystallographic c-axis Maximum expansion is achieved for C_8Cs at 1.78.

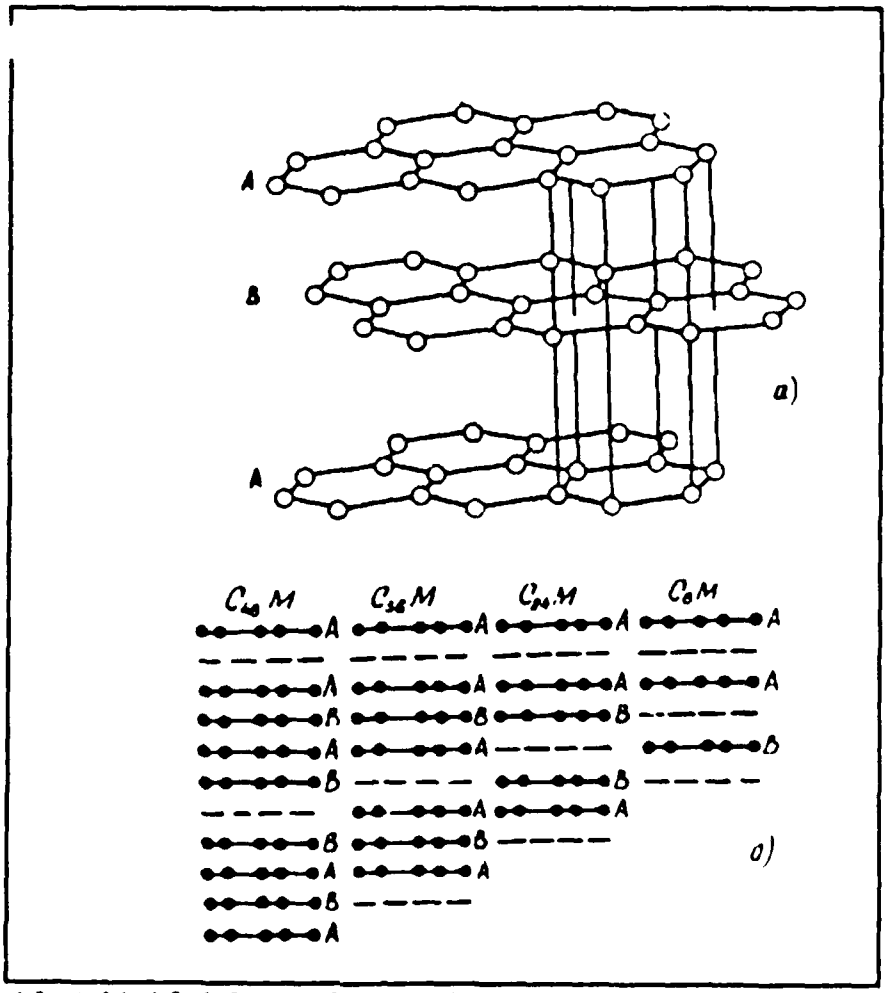

Figure 4 3 a) Modified Graphite Hexagonal Lattice, b) Schematic Representation of Phase Structures of the Cs-Graphite System

It is not known what the situation looks like at the surface of the graphite We suspect, however, that positive Cs ions may be present at the surface These positive ions (versus the normal neutral atom of adsorbed cesium present for a metal electrode) could create a very localized negative electron affinity, or at least a very low positive affinity, as shown in Figure 4 4 This may contribute toward the excellent results obtained for cesiated graphite

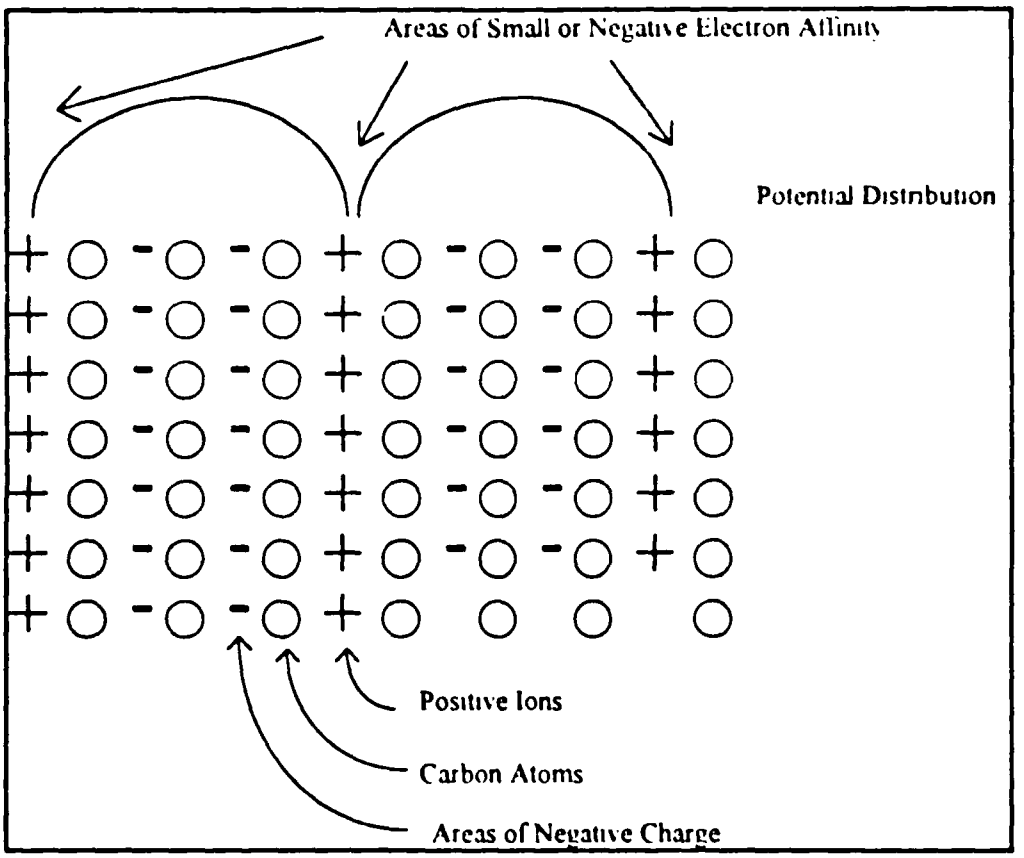

Figure 4 4 Hypothesized Potential Distribution in Cs-Graphite System

Cesium-intercalated graphite is stable for moderate times in air at ambient temperature Therefore handling of cesium-intercalated graphite does not present a serious problem from the standpoint of manufacturing

MANUFACTURABILITY OF INTERCALATED FIBER CATHODES

Surprisingly, other groups have investigated the use of carbon fibers for the purpose of cathode fabrication [2] Of maximum interest is the work of a group at the Institute of Cybernetics Problems, Russian Academy of Sciences Chakhovskoi et al have been pursuing the fabrication of carbon fiber individual cathodes for flat panel indicators and have already achieved a limited measure of success As shown in Figure 4 5,

individual or groups of fibers can be contained in a metal jacket. Individual fibers may be as small as 4 μ.

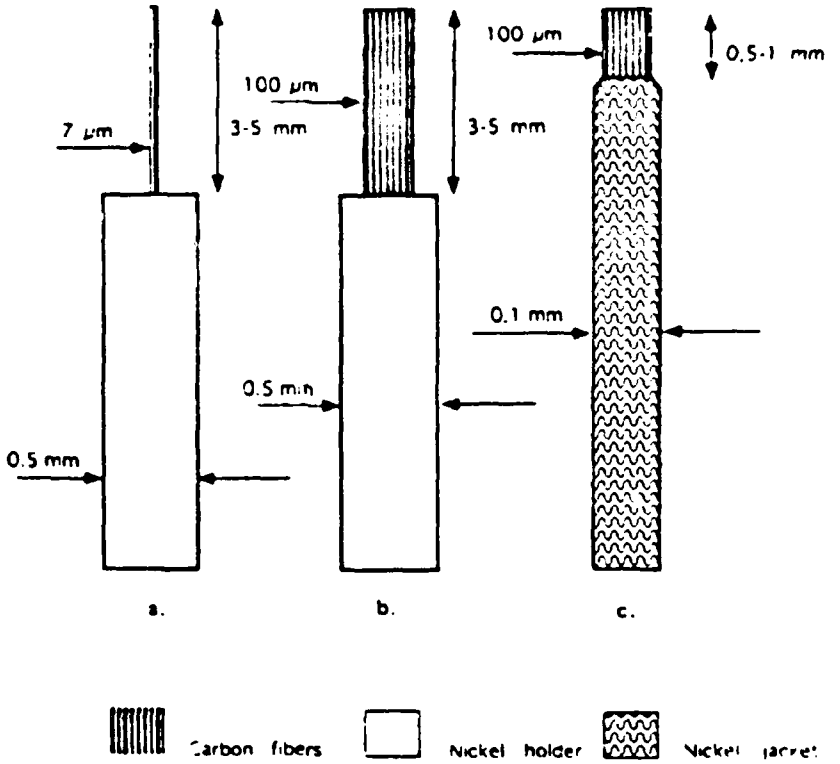

Figure 4.5 Carbon Field Emitters: (a) 7 μ single fiber; (b) 100 μ bunch of fibers; (c) 100 μ bunch in a 0.1 mm nickel jacket deposited by magnetron sputtering.

The field emitters in nickel holders are placed into a fluoroplastic frame. After solidification of the dielectric, the fluoroplastic frame is removed. Then the matrix blank is filled with a liquid dielectric material and baked to harden the dielectric. The matrix blank is then machined with electric discharge machining (EDM) to ensure uniformity of emitter dimensions. The final appearance of the matrix carbon field array is shown in Figure 4.6.

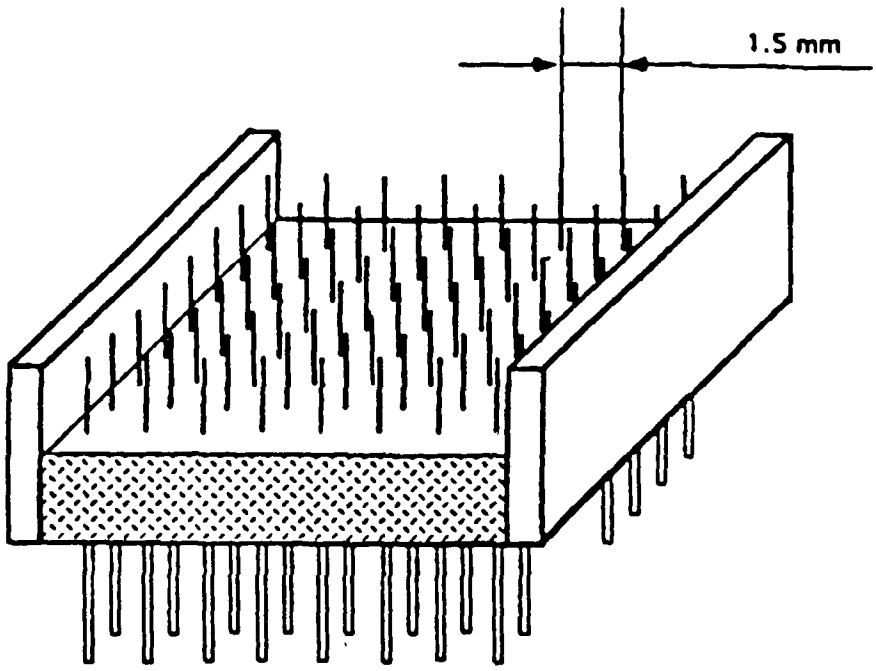

Figure 4.6 Final View of Matrix Field Cathodes.

Obviously, to be attractive for video display applications, such cathode arrays must be miniaturized, and must use carbon fibers which are ideal for intercalation. Such fibers are likely to be found in the form of vapor grown carbon fiber or VGCF.

Commercially available carbon fibers are filaments with diameters of five to fifteen microns, consisting of axially aligned graphitic carbon. These fibers are manufactured by the controlled pyrolysis of spun organic polymeric precursor material. The extraordinary mechanical properties of commercial carbon fiber are due to the unique graphitic morphology of the spun filaments.

VGCF is produced by a catalytic process from hydrocarbon gas. The purity of the carbon source and the mechanics of growth result in a highly graphitic fiber with a unique lamellar morphology and physical properties approaching those of single-crystal graphite. Single-fiber properties of VGCF are summarized in Table 4.1 below.

Table 4.1 Properties of ASI VGCF

Filament Diameter	Submicron to >100 microns
Tensile Strength	7.0 (1000) GPa (ksi)
Tensile Modulus	600 (87) Gpa (Msi)
Break Elongation	0.5 %
CTE	-1.0 ppm/°C
Density	2.1 g/cm^3
Electrical Resistivity	55 μO cm
Thermal Conductivity	1950 W/mK @ 300 K

Figure 4.7 is a scanning electron microscope image of a VGCF filament revealing its highly graphitic structure. VGCF is easily graphitized due to its unique morphology (figure 2), and the purity with which carbon is incorporated into the crystal lattice.

VGCF is basically planar graphite which is wrapped into cylinders (sometimes referred to as "buckytubes"). The lattice is very well ordered and offers extremely high thermal conductivity. The electrical conductivity of intercalated graphite fibers is as high as many metals. Thus, this form of graphite is an are excellent candidate for intercalation and incorporation into a cathode array at the microscopic level required for practical video display cathodes.

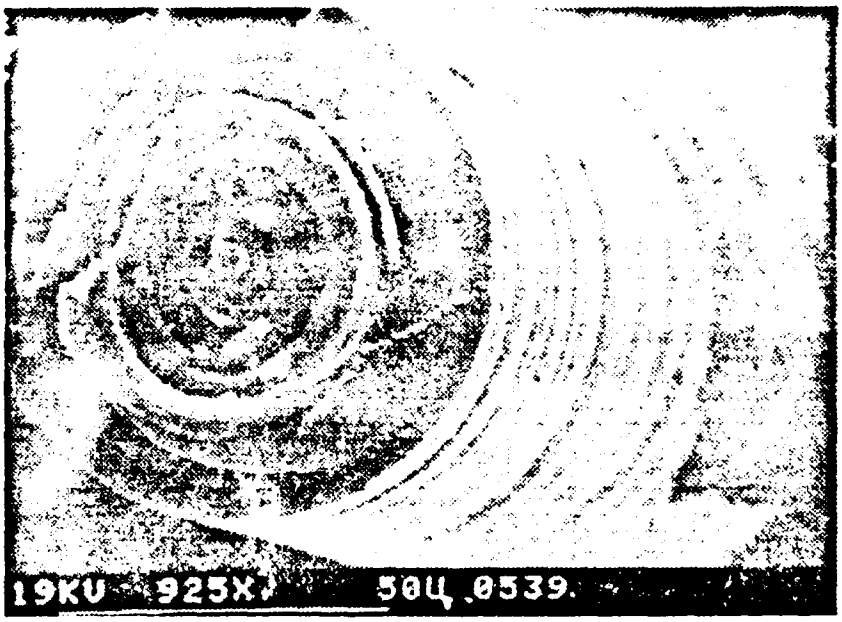

Figure 4.7 SEM Micrograph of VGCF

The procedure used to produce the form of VGCF referred to as Pyrograf™ I is a three stage batch process, consisting of a reduction stage, a fiber growth stage, and a fiber thickening stage.

The first stage is reduction of the catalyst, which is supported on a substrate, in a hydrogen atmosphere. Following the reduction stage, the gas flow is changed to a mixture of methane and hydrogen in a linearly increasing temperature sweep to 1100° C. Fibers are nucleated and elongated as methane decomposes on the catalyst, m and the catalytic particle migrates down the reactor in the direction of gas flow. The fibers lengthen at a rate of approximately 3 millimeters per minute. In the third stage, the gas mix is enriched with methane, allowing for the thickening of the fiber through chemical vapor deposition of carbon on the surface of the fiber. The resulting fibers can thus be produced with selected lengths and diameters, depending on the time of growth and thickening, and on the gas mixtures and flow rates. This fiber grown on any surface which is seeded with catalyst. Typically several graphite boards are seeded and stacked a tube

furnace. Fiber grown on the top of a board is harvested as a semi-woven mat resembling a veil or paper. Fiber growing from the bottom of a board hangs down due to the pull of gravity and is harvested as sheets resembling fur or hair.

A second commercial variety of VGCF has been developed and is identified as Pyrograph™ III. This material has been developed with the aim of eliminating the need for supporting the catalyst and for cooling the furnace prior to removing the fibers and their supports. Instead of supporting the catalyst on a surface within the furnace, the catalyst is formed, nucleates, and grows a fiber within the gas phase. Due to the shorter length of time that the growing fiber remains in the furnace, the diameter and length is much smaller than those of Pyrograph I. Since the fiber is entrained in the gas flow, it is easily blown out of the furnace without stopping the process and cooling the furnace. In the batch process, the majority of the process time is the heating and cooling of the furnace. The continuous process eliminates these times and greatly increases the efficiency.

The novel method by which VGCF is produced thus holds promise for substantially improving the physical properties, particularly the thermal conductivity, of composite materials, as well as for designing even higher performance materials through chemical vapor deposition (CVD), addition of dopants, and surface treatments. Figure 3 shows the mass specific thermal conductivity of VGCF compared to other candidate materials used in thermal energy management components, and figure 4 shows the specific thermal conductivity which has been achieved to date on undensified VGCF preforms.

Although extensive data on single fiber properties of VGCF have been determined through fundamental research studies, no manufacturer of large volumes of VGCF exists in the United States, and as a consequence almost no physical property data are available for VGCF composites. Three major companies in Japan are known to be pursuing some type of VGCF production. This is significant in view of the fact that Japan currently produces a large majority of the worldwide supply of carbon fiber, and that the U.S. composites industry is thus highly dependent on foreign producers of fiber.

References

1. A. G. Kalandarishvili, *Working Medium Sources for Thermionic Power Converters*, Energoatomizdat, Moscow 1993.

2. A. G. Chakhovskoi, et al., "Method of Fabrication of Matrix Carbon Fiber Field Emission Cathode Structures for Flat-Panel Indicators," Journal of Vacuum Science Technology B 11 (2), Mar/Apr 1993.

V. CONCLUSIONS

This effort successfully demonstrated that intercalated graphite fibers are outstanding cathode materials. Such fibers are staole in air at ambient temperature and offer current densities of over 100 Amps/cm^2 at 10 volts bias voltage (at 700 K). Ambient temperature cathodes also offer high current capability at somewhat higher bias voltage.

The effect is now presumed to be the result of the formation of cesium intercalation compounds, which present positive cesium ions near the surface of the graphite cathode (oriented such that the graphitic planes are parallel to the emission direction).

Our original postulate that this is due to a negative electron affinity condition, which can exist in diamond as well as graphite, is incorrect. We now believe that good results from diamond are due to the presence of graphitic inclusions between individual grains of diamond. These graphitic inclusions are able to interact with cesium.

Intercalated graphite is relatively stable in air for moderate durations and can be handled without difficulty. Thus the cathodes we are describing *do not require* a cesium reservoir in order to function.

Long term stability against cesium leakage is an issue, but we believe that this can be simply handled by using relatively high voltages and only moderate temperatures in order to achieve the enhanced emission. Future research should concentrate on developing the performance at ~100 °C or less, with bias voltages of 100 volts or possibly a little higher.

Technology is now being developed to utilize micron-sized fibers in cathode arrays which could have definite applications for video displays. The discovery that intercalated graphite fibers offer orders-of-magnitude improved performance is very important to this research.